Universität Hamburg
DER FORSCHUNG | DER LEHRE | DER BILDUNG

Master's thesis

Retrieval of Attenuation and Reflectivity in a Networked Radar Environment

Submitted by	**Finn Burgemeister**
Students Id	6650507
Course of studies	Meteorology

Date	February 20, 2020

First supervisor	Prof. Dr. Felix Ament
	Meteorological Institute
Second supervisor	Dr. Marco Clemens
	Meteorological Institute

Topic of this thesis:

Retrieval of Attenuation and Reflectivity
in a Networked Radar Environment

Abstract

Radar measurements are attenuated significantly, especially at short wavelengths, e.g. X-band and K-band. For the intersecting observations of weather radars operated in a networked environment, a novel retrieval method for reflectivity and specific attenuation estimates is developed. The retrieval method derives an linear system of equations (LSE) based on the observed radar reflectivities considered as tomographic problem. A major advantage of this LSE-method is the independence of explicit constraints, like statistical relations of the k-Z-relation.

The retrieval algorithm is tested using synthetic weather radar data to prove the validity and sensitivity of the method. The sensitivity of the LSE-method is discussed for several uncertainties: local perturbations, noise, missing values, biases, different number of radars, and strong attenuation. Especially a noise significant greater than the specific attenuation and biases between the observed reflectivities corrupt the retrieval's solution. Nevertheless, the LSE-method is found to be applicable to synthetic data of weather radar networks considering the underlying assumptions of the observations and methodology.

The application of the LSE-method on real radar data shows inconsistency to the theoretical assumptions. The real observations are provided by several single polarised X-band weather radars operated in a unique network design. The spacious measurements of the networked radars are incomparable. The scanning strategy and vertical inhomogeneity of the reflectivity lead to different simultaneous reflectivities. Consistently, the application of the LSE-method to retrieve reflectivity and specific attenuation is constrained to a weather radar network operating at zero elevation or connecting lines. Additionally, ground clutter and strong attenuation causes missing values in the observations leading to the underestimation of the path integrated attenuation.

However, the fundamental analysis of the presented method to retrieve reflectivity and specific attenuation in a weather radar network proves its theoretical validity. Nevertheless, further research on attenuation correction schemes for weather radars operating at small wavelengths and in networks is needed.

Kurzfassung

Insbesondere bei kurzen Wellenlängen, z.B. X- und K-Band, werden Messungen der Radarreflektivität signifikant durch Flüssigwasser gedämpft. Aus den sich überschneidenden Beobachtungen von mehreren Wetterradaren wird ein neues Verfahren zur Bestimmung der spezifischen Dämpfung und somit einer Korrektur der Radarreflektivität entwickelt. Die Methode leitet ein lineares Gleichungssystem (LSE) aus den beobachteten Reflektivitäten der Radare her. Der Vorteile der LSE-Methode ist die Unabhängigkeit von Einschränkungen, wie die statistischen Zusammenhängen einer k-Z-Beziehung.

Das Verfahren zur Ableitung der spezifischen Dämpfung und wahren Reflektivität wird anhand synthetischer Wetterradardaten getestet, wodurch die allgemeine Gültigkeit und Sensitivität der Methode gezeigt werden. Die Sensitivität der LSE-Methode wird für verschiedene Unsicherheiten diskutiert: lokale Störungen, Rauschen, fehlende Werte, Bias, Anzahl der Radare und starke Dämpfung. Das Ergebnis der Methode wird insbesondere durch Rauschen gestört, das in der Größenordnung signifikant größer als die Werte der spezifischen Dämpfung ist. Unterschiedliche Beobachtungen, durch beispielsweise einen Bias in der Kalibration, führen ebenfalls zu einer instabilen Lösung. Unter Beachtung der Annahmen der Beobachtungen und der Methodik, führt die LSE-Methode zu einer robusten Abschätzung der Radarreflektivität und spezifischen Dämpfung.

Die Anwendung der LSE-Methode auf reale Radardaten zeigt widersprüchliche Ergebnisse zu den theoretischen Annahmen. Die realen Daten basieren auf den Beobachtungen eines Niederschlagsereignisses von mehreren einfach-polarisierten X-Band Wetterradaren in einem einzigartigen Netzwerkaufbau. Die großflächigen Messungen der Radare im Netzwerk sind jedoch nicht vergleichbar. Die Messstrategie und vertikale Inhomogenität der Radarreflektivität führt zu verschiedenen beobachteten Reflektivitäten für gleiche Standorte. Die LSE-Methode lässt sich folglich nur für horizontal messende Wetterradare anwenden. Nicht-meteorologische Echos und starke Dämpfung verursachen zudem fehlende Beobachtungswerte.

Die grundlegende Analyse der vorgestellten Methode zur Ableitung der ungedämpften Radarreflektivität und spezifischen Dämpfung aus Beobachtungen eines Wetterradarnetzwerks zeigt die theoretische Gültigkeit. Die vertikale Variabilität der physikalischen

Eigenschaften und Messungenauigkeiten verhindern die praktische Anwendung. Die Zukunft erfordert weitere Forschung im Bereich der Dämpfungskorrekturen für Wetterradare, die in kurzen Wellenlängen messen und in Netzwerken eingesetzt werden.

Contents

List of Acronyms **X**

1 Introduction **1**

2 Background **5**

2.1 Weather Radar Network 5

2.2 Attenuation 7

3 Method for Network Based Retrieval **11**

3.1 Radar Forward Operator 12

3.2 Methodology 14

3.3 Inverse Problem's Solution 16

4 Experimentation of the Retrieval Algorithm on Synthetic Radar Data **19**

4.1 Methodology 19

4.2 Data 21

4.3 Retrievals 25

5 Application of the Retrieval Algorithm on Real Radar Data **39**

6 Conclusion and Outlook **49**

Bibliography **51**

List of Figures **55**

List of Acronyms

BKM	Bekmünde
clutter	non-meteorological echoes
DSD	raindrop size distribution
DWD	Deutscher Wetterdienst
HWT	Hungriger Wolf Tower
LSE	linear system of equations
MOD	Moordorf
MRR	Micro Rain Radar
PATTERN	Precipitation and Attenuation Estimates from a High-Resolution Weather Radar Network
PIA	path-integrated attenuation
QNS	Quarnstedt
RMSE	root-mean-square error
WST	Itzehoe

1 Introduction

High resolution weather radars are mandatory for spacious precipitation estimates needed in several meteorological and hydrological applications at small scales. The increase in extreme rainfall events due to climate change drives the development in urban hydrological models, which demand high quality and resolution inputs (Thorndahl et al., 2017). Conventional weather radar systems, operating at S- and C-band frequencies, are able to provide reflectivity measurements over large domains, but are limited in temporal resolution of several minutes and spatial resolution of a few hundred meters. However, different hydrological applications demand at least a temporal resolution of 1 min and spatial resolution of 100 m (Einfalt, 2003; Ochoa-Rodriguez et al., 2015; Thorndahl et al., 2017). With smaller wavelengths, for example at X-band frequencies, a weather radar has a beneficial gain in sensitivity of the signal and resolution, but suffers from attenuation by water significantly. This effect of attenuation is neglibile at wavelengths in the S-band range. In general the knowledge of attenuation is important for two reasons. First, the specific attenuation k is used to correct the measured radar reflectivity Z. The retrieval of intrinsic reflectivity is a prerequisite for rain rate R estimates, especially in heavy rain events. Second, the knowledge of specific attenuation is useful at its own since the rain rate can be estimated directly from this property using so-called k-R relationships (Doviak and Zrnić, 1993). The attenuation of microwaves by rain has been discussed and used for nearly seven decades (Atlas and Banks, 1951; Atlas and Ulbrich, 1977; Austin, 1947; Gunn and East, 1954; Wexler and Atlas, 1963; to mention some of the earliest).

As attenuation is known as essential problem for radar measurements, there is a wealth of techniques and algorithms to correct the effect of attenuation. Initially, Hitschfeld and Bordan (1954) derived an analytical function for the rain rate depending on the observed signal power using familiar Z-R and k-R relations as attenuation correction. The application of this scheme is limited due to its dependencies and the sensitivity to calibration errors. Therefore, Hildebrand (1978) enhanced the analytical function by an iterative solution for attenuation correction restricted to an attenuation underestimation. Both algorithms get unstable for small errors and increasing path-integrated attenuation (PIA) (Delrieu et al., 1999; Peters et al., 2010). The schemes are improved by constraints of the PIA to avoid the overestimation of attenuation due

to instability (Delrieu et al., 1999; Marzoug and Amayenc, 1991; Nicol and Austin, 2003). Further, dual-polarised radars improve data quality by estimating the attenuation through using the differential phase (Feng et al., 2016), but single-polarisation systems are preferred because of their low costs. In summary, attenuation correction schemes for single radars are limited in applicability especially for strong rain events.

As most weather radars are used in nationwide, large or local networks they provide more coverage and can improve the rain estimate with different observations about overlapping areas. The supplementary use of X-band weather radar systems to conventional weather radar networks at local scales, i.e. urban areas, has been tested at different sites (Antonini et al., 2017; Chandrasekar et al., 2018; Cifelli et al., 2018; Lengfeld et al., 2014; Van de Beek et al., 2010). Multiple observations by different radars are used to improve the rain estimate. For example, Lengfeld et al. (2016) introduced a method to correct reflectivity measurements of weather radars operating in attenuation-influenced frequency bands using observations from less attenuated radars. A different way to increase the accuracy of the corrected reflectivity is using C-band radar observations to restrict familiar single radar attenuation corrections of X-band radar measurements (Lengfeld et al., 2018). For weather radars operating at the same frequency band, Testud and Amayenc (1989) presented an attenuation retrieval using two radars observing a common volume. Since the concept is based on a second-order differential equation, it is highly sensitive to noise of the measured variables. With an improved formulation of this differential equation, the attenuation correction was applied for measurements at same level performed during several flights with a dual-beam airborne Doppler radar including an independent evaluation with ground based radar measurements (Kabèche and Testud, 1995). Srivastava and Tian (1996) discussed a dual-radar method of measuring specific attenuation at virtually the same wavelength with an analytical solution. The technique was successfully applied to C-band observations (Tian and Srivastava, 1997), but this study lacks independent measurements of specific attenuation to verify the validity of the retrievals. Chandrasekar and Lim (2008) proposed an iterative methodology for reflectivity and specific attenuation retrievals in a networked radar environment. The method is based on the solution of the specific attenuation distribution by the integral equation for the reflectivity factor. The network-based attenuation correction algorithm works robustly for simulated X-band observations by using a S-band radar (Chandrasekar and Lim, 2008) and real X-band radar observations (Lim et al., 2011). Disadvantages of the method are the computationally intensive solution and a required parameter of the Z-k relation. The most recent method related to the retrieval of specific attenuation by multiple radar observations, presented by Shimamura et al. (2016), is based on the maximum likelihood estimation for the solution of the analytical function by Hitschfeld and Bordan (1954).

Overall, research on attenuation correction schemes for weather radars operating at small wavelengths has not yet been completed.

Several studies show the capability of weather radar networks improving rain estimates (Lengfeld et al., 2018, 2016; Lim et al., 2011; Shimamura et al., 2016). As weather radar networks provide multiple information about same measuring volumes, they can overcome the drawback of attenuation. Therefore, the project Precipitation and Attenuation Estimates from a High-Resolution Weather Radar Network (PATTERN) provided a well-grounded testbed for research on high-resolution weather radar measurements (Lengfeld et al., 2014). The integrated X-band weather radars provide years of measurements. The network design promotes the idea of a networked approach to correct the influence of attenuation.

This thesis encompasses the development and exploration of a novel retrieval method for reflectivity and specific attenuation estimates in weather radar networks. The focus is on observations by short wave, single polarised weather radars in an unique network design, as described in Chapter 2. The networked observations are considered as a tomographic problem. To introduce the theoretical framework for a novel networked based retrieval method in Chapter 3, the theoretical background of attenuation is given in Chapter 2. Experimentation on synthetic weather radar data demonstrates assets and drawbacks of the retrieval method in Chapter 4. Finally, the usability of this method is discussed using real weather radar data (Chap. 5). The potential and limitations of the presented retrieval method is summarised in Chapter 6.

2 Background

In general, a weather radar transmits microwaves, which are partially backscattered by hydrometeors, e.g. cloud droplets, raindrops, snowflakes, and hailstones. The reflectivity, as the result of this backscattered signal, is affected by attenuation, in part very significant depending on the wavelength (Sec. 2.2). A setup of multiple radars operated in a networked environment provides not simply measurements over long ranges but can also overcome the drawback of attenuation (Sec. 2.1).

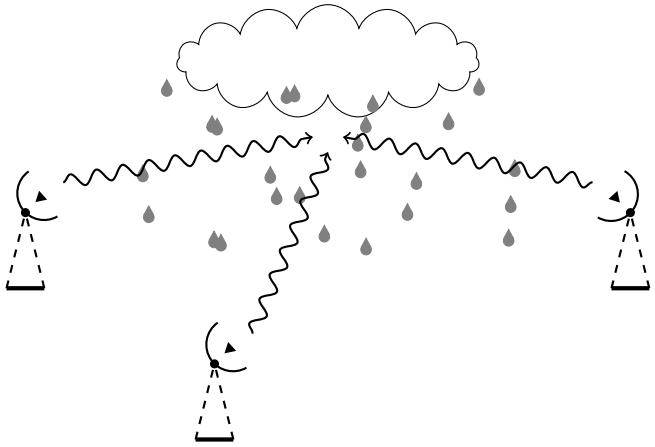

Figure 2.1: Sketch of a radar network observing the same volume.

2.1 Weather Radar Network

A weather radar network, consisting of two or more radar systems, provides multiple information about the same measuring volume characterised by one raindrop size distribution (DSD), describing the microphysical properties of the rain medium. The observed reflectivities on common volumes are distinct due to the different propagation paths of the signals by each radar (Fig. 2.1). Each radar beam is affected by a variety of different specific attenuations due to an inhomogeneous rain field, leading to a radar dependent *PIA*. Nevertheless, one volume has one intrinsic reflectivity and specific attenuation. Even though the radar beams just intersect in parts, these multiple observations can be used to improve the rain estimate.

Within the project's framework of PATTERN, a weather radar network had been set up with the aim to overcome the drawback of attenuation and improve accurate

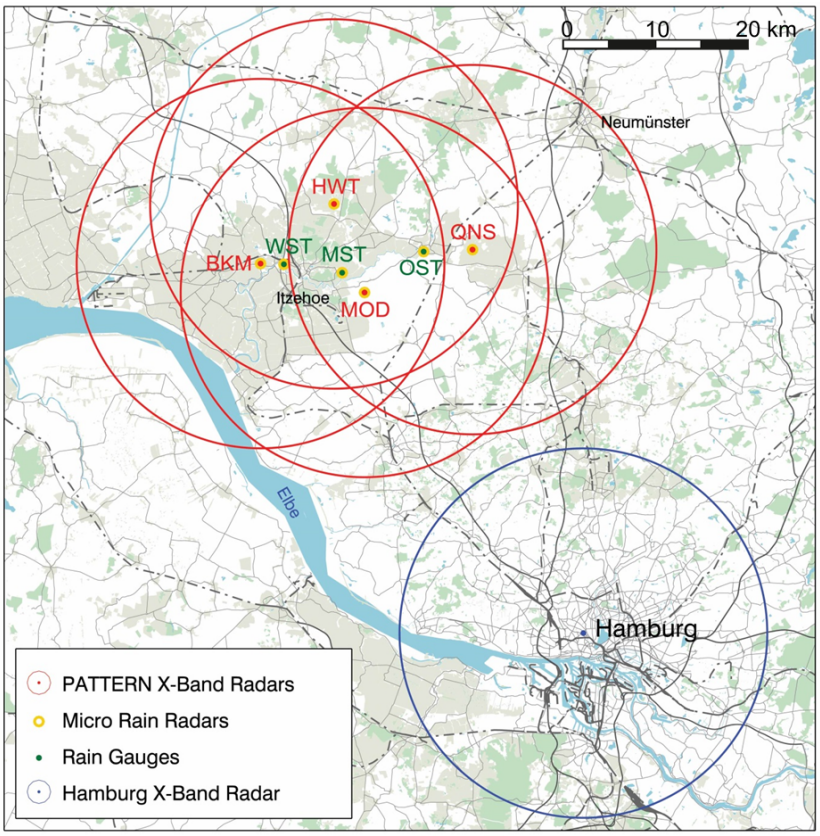

Figure 2.2: Map of weather radar network PATTERN (Lengfeld et al., 2014).

quantitative precipitation estimates (Lengfeld et al., 2014). The network consists of four X-band radars, three Micro Rain Radars (MRRs) and several rain gauges. The setup was located in the north of Hamburg, Germany (Fig. 2.2). Supplementary, the whole radar network is covered by observations of the C-band Doppler radar in Boostedt of the Deutscher Wetterdienst (DWD). Each X-band radar has a maximum range of 20 km, a range resolution of 60 m and a time resolution of 30 s. The radars, Hungriger Wolf Tower (HWT), Bekmünde (BKM), Moordorf (MOD), and Quarnstedt (QNS), span an observed region of approximately 60 km $\times$ 80 km. The radar systems are modified ship navigation radars with 25 kW transmit power, a frequency of 9410 MHz (X-band frequency range is $8-12$ GHz), a pulse width of 0.4 μs and a pulse repetition frequency of 800 Hz. Each radar has a sampling resolution of 1° in azimuth and operates with an elevation angle of roughly 3° (Burgemeister, 2018). For further technical details see Lengfeld et al. (2014).

Although the X-band radars are single polarised and thus they lack of polarimetry added-values, the radars provide benefit from the advantages of low costs and the other X-band and vertical pointing MRRs, or more exactly the networked setup. The unique character of this network is worth emphasising because the horizontal distance of any two radars does not exceed 16 km. As a result, the radar observations overlap in the

full propagation paths of the radar beam, even though in different heights. This condition is also fulfilled for a network of three out of four radars. The overlap of the PATTERN weather radar observations is greater in percentage terms compared to the nationwide C-band network by the DWD. With this network and an appropriate approach the multiple information from different radars can be used to retrieve reflectivity and attenuation in certain grid cells.

For the network within PATTERN, several attenuation correction approaches using different radars have been tested. Note that, attenuation effects due to a wet radome during rain events are minimised with the cylindrical shape of the X-band radar's radome because water runs off quickly (Lengfeld et al., 2014). Peters et al. (2010) introduced a spectral attenuation correction for the MRR based on the scheme by Hitschfeld and Bordan (1954). Attenuated X-band radar's measurements are successfully corrected for a single case by Lengfeld et al. (2014) using the single radar attenuation correction scheme by Delrieu et al. (1999) with a constrained *PIA* and fixed parameters. The attenuation is estimated along the path of undisturbed radar measurements. Data gaps due to clutter removal are filled by interpolation or, if possible, by multiple radar information in overlapping areas. Additionally, within PATTERN Lengfeld et al. (2016) proposed a method to correct attenuation-influenced radar observations with by less attenuated radar observations. The attenuation of the X-band radar observations are corrected with the measurements of C-band radars by using an isotonic regression applied on the ratio between these measurements. This method and five more attenuation correction methods are examined and compared by Lengfeld et al. (2018). Despite all attenuation correction methods lead to improvements, single radar schemes tend to instabilities. Additionally, the dual radar (X- and C-band radar) scheme is uncertain in terms of different time resolutions (30 s to 5 min) and unknown differences due to different beam heights.

As the goal of this thesis is a retrieval of reflectivity and attenuation in a weather radar network, discussed ideas of a theoretical and the real weather radar network (PATTERN) are considered. To develop the network based retrieval, some thoughts about attenuation are given in Section 2.2.

2.2 Attenuation

The scattering and absorption of the emitted and reflected electromagnetic wave propagating in precipitation is called attenuation. The power loss of the backscattered signal due to attenuation leads to strongly underestimated reflectivities and thus rain estimates. The attenuation at short wavelengths, e.g. at X-band, can be 100 times larger than at longer wavelengths, like S-band, where attenuation can be approximately ne-

glected (Doviak and Zrnić, 1993). The effect of attenuation increases with strong rain and at long ranges. Due to this cumulative characteristic of attenuation, observations from multiple sites measure different reflectivities, which leads to different rain estimates. Therefore, an attenuation correction for the radars described in Section 2.1 is mandatory. To introduce the retrieval method in Chapter 3, a brief overview about important radar quantities is given.

The measured logarithmic radar reflectivity Z' at range r suffers from attenuation integrated over the path, neglecting noise and non-meteorological echoes (clutter),

$$Z'(r) = Z(r) - 2\int_0^r k(s)\,\mathrm{d}s \tag{2.1}$$

where $Z(r)$ is the intrinsic logarithmic radar reflectivity at range r and $k(s)$ is the specific attenuation of each range bin. The integral in Equation 2.1 is also known as *PIA*.

The intrinsic linear radar reflectivity z in the unit of $\mathrm{mm^6 m^{-3}}$ can be expressed at any range bin r as a function of the DSD $N(D, r)$ and the drop size itself D:

$$z(r) = \int_0^\infty N(D, r) D^6\,\mathrm{d}D. \tag{2.2}$$

The units of the linear radar reflectivity z in $\mathrm{mm^6 m^{-3}}$ is transferred to the logarithmic radar reflectivity Z in dBZ using

$$Z = 10 \cdot \log_{10}(\frac{Z}{z_0}) \tag{2.3}$$

where $z_0 = 1\,\mathrm{mm^6 m^{-3}}$. Unless otherwise stated, for simplicity, the logarithmic radar reflectivity is expressed as radar reflectivity in the following.

The formulation for the specific rain attenuation k in the unit of $\mathrm{dB\,m^{-1}}$ can be expressed similar to the radar reflectivity (Eq. 2.2)

$$k(r) = 4.34 \cdot 10^{-3} \int_0^\infty N(D, r)\sigma_\mathrm{e}(D)\,\mathrm{d}D \tag{2.4}$$

where $N(D, r)$ is the DSD and σ_e is the extinction cross section, which is dependent on the wavelength. To obtain the wanted rain estimates, the linear radar reflectivity z has to be converted into a rain rate R, usually by assuming a power law $z = a\,R^b$. The issue is that the coefficients a and b are not constant in space and time and depend on e.g. the type of precipitation (Berne and Krajewski, 2013). For a further description of radar background refer to standard literature, e.g. Doviak and Zrnić (1993).

As the radars described in Section 2.1 are simple backscatter systems and cannot observe Doppler shift or perform polarimetric measurements (Lengfeld et al., 2014),

they provide only the radar reflectivity. For this reason, a retrieval method based on Equation 2.1 without using microphysical properties of the rain medium, like the DSD, is presented in Chapter 3.

3 Linear System of Equations Method for a Network Based Retrieval - Theory

The basis of any networked retrieval method for attenuation and reflectivity is to observe common volumes. Imagine a hypothetical radar network observing same areas at different radar sites simultaneous (Fig. 2.1). The measurements are considered to be in a plane, so connecting lines and intersecting volumes are extensively possible (Fig. 3.1). The vertical microphysical properties of the precipitating area are assumed to be approximately constant or the elevation angle of the radars nearly zero. The hypothetical radars are operating at the same frequency band. The radar beam is considered as a pencil beam after the correction of power loss due to a beam expansion effect. The geometry is simplified to neglect a mismatch in range resolution volume and pointing regarding overlapping measurements by different radars, hence the measurements are discretised on same grid nodes. In absence of attenuation, the measured radar reflectivity is assumed to be the same for common nodes. Nevertheless, the observation of intrinsic reflectivity for a common node is distinct due to different integrated attenuation along the paths from each radars and additional uncertainties.

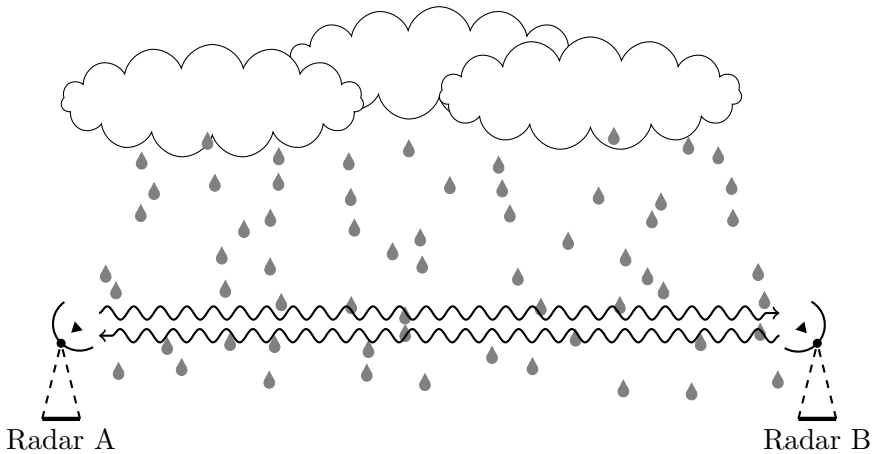

Figure 3.1: Idealised set up of a radar network along connecting lines consisting of two radars A and B.

The methodology for the following network based retrieval of attenuation and reflectivity is based on a linear system of equations (LSE) derived from Equation 2.2, which

relates the measured reflectivity Z', the intrinsic reflectivity Z and the specific attenuation k integrated over the beam path. As the observations are available on a radial grid with its centre in each radar location, the measurements have to be interpolated on the same regular grid nodes, e.g. of Cartesian coordinates. Therefore, Equation 2.2 has to be discretised according to the selected grid to describe the propagated beam path. The radar forward operator is used for the discretisation, which is described in Section 3.1. The general methodology of the retrieval method, the LSE, is introduced in Section 3.2. Schemes to solve the LSE are discussed in Section 3.3.

3.1 Radar Forward Operator

The radar forward operator simulates the observed logarithmic reflectivity Z' for a given spatial distribution of intrinsic logarithmic reflectivity Z and specific attenuation k. All fields, for instance Z', are discretised by a basis function. This approach is inspired by the finite element method. Consider N nodes of $\{P_i \,:\, 1 \leq i \leq N\}$ inside the two-dimensional model domain with a triangulation consisting of four triangles per node (Fig. 3.2a). This nodal basis ϕ_i is given by a function, which varies linearly within each triangle and fulfils

$$\{\varphi_i \,:\, \varphi_i(P_j) = \delta_{ij}\} \tag{3.1}$$

with the Kronecker delta δ_{ij}. A hypothetical field x is then discretised by these elements φ_i:

$$x(\vec{r}) = x_i \varphi_i(\vec{r}) \tag{3.2}$$

with the scalar coefficients x_i, which are easily determined by the relation $x(P_i) = x_i$. To shorten the notation, the nodal coefficients x_i are summarised into the vector $\vec{x} = (x_1, ..., x_N)$. It is straightforward to restrict the model to one dimension for studies of anti-axially looking radars (Fig. 3.1), by replacing the triangulation with an intersection of the connecting line into intervals (Fig. 3.2b).

Following the defined notation, the measured reflectivity $Z' = (Z'(x_1), ..., Z'(x_N))$ of the indicated radar in Figure 3.2 is computed following Equation 2.2:

$$\vec{Z}' = \vec{Z} - 2\,\mathbf{B}\,\vec{k} \tag{3.3}$$

with the discretised intrinsic radar reflectivity $\vec{Z}$, the specific attenuation $\vec{k}$ and a beam matrix $\mathbf{B}$. The beam matrix $\mathbf{B}$ describes the geometry of the radar beam and is therefore time independent. The elements $\mathbf{B}(i, j)$ of the matrix are calculated integrally

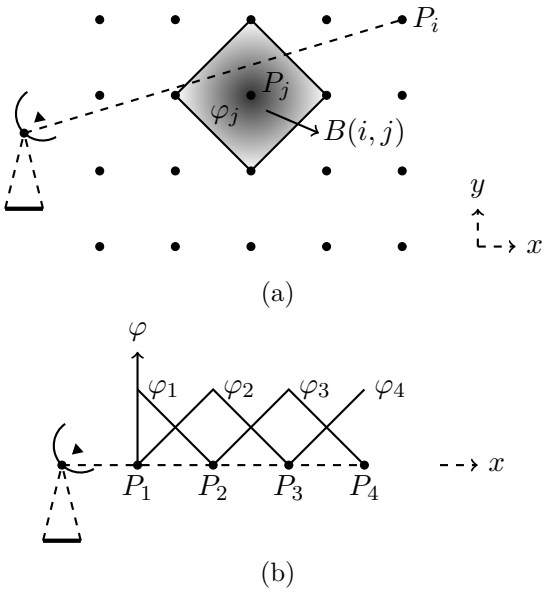

Figure 3.2: Discretisation of horizontal, two-dimensional (a) and one-dimensional (b) fields using nodal basis functions. The nodes are indicated by the dots P and the basis function is denoted by the functions φ, which is in (a) the shaded area.

over the nodal basis functions ϕ_j:

$$\mathbf{B}(i,j) = \frac{l_i}{c_i} \int_{L_0}^{P_i} \varphi_j \, \mathrm{d}s \tag{3.4}$$

$$l_i = \int_{L_0}^{P_i} \mathrm{d}s, \qquad c_i = \sum_j B(i,j) \tag{3.5}$$

within the path ($[s] = \mathrm{m}$) between the radar location L_0 and the directed node P_i. The beam matrix is of dimension $N \,\mathrm{x}\, N$. The values of the line integrals are standardised by c_i with the sum of the weights affecting the beam path and by l_i with the length of the beam path (see Eq. 3.4 and 3.5). This normalisation is required due to a discretisation error, which is indicated in Figure 3.3. For the case that the radar beam is parallel to the nodes, the normalisation changes nothing. The integral of the basis functions ϕ_i over the full path s results in the path length due to the intersection of the functions (Fig. 3.2b). The normalisation becomes essential for a radar beam, which is nonparallel to the nodes, as the line integral of the basis functions would not maintain the propagated beam path. A diagonal beam according the node results with its line integral of ϕ_i in a discretisation error with a factor of the square root of two. In this case, the weight functions are separated (Fig. 3.3). Note, if the finite element method is applied, the discretisation error will be minimised by variation of the basis function with each node. However,

the finite element method was not applied by this approach. The normalisation with Equation 3.5 resolves this issue. On the bottom line of the discretisation, the entries of the beam matrix are just the scaled lengths of the ray paths corresponding to the nodes.

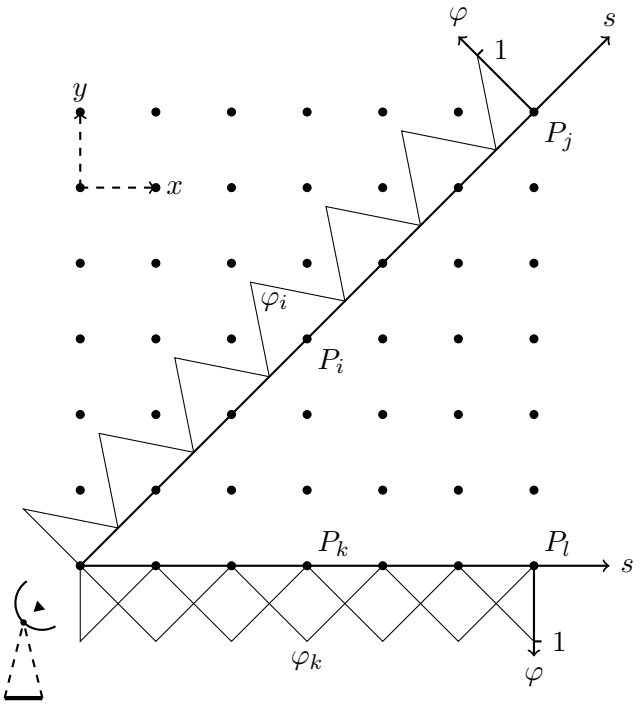

Figure 3.3: Explicit weighting of two exemplary beam paths on a two-dimensional field using the nodal element basis. The nodes are indicated by the dots P and the basis functions are denoted by the functions φ.

The radar forward operator (Eq. 3.3) derived from Equation 2.2 allows the description of the measured reflectivity Z' in relation to the intrinsic reflectivity Z and specific attenuation on a regular grid. It is important to note that the measured reflectivity in Equation 2.2 as well as Equation 3.3 depends on the *PIA* and thereby includes the full radar beam starting from the radar site. Placing the radar outside of the model domain results in an underestimation of the *PIA* due to missing nodes, which are affected by specific attenuation nevertheless. The modeling of the measured reflectivity with the radar forward operator enables the methodology of a retrieval method (Sec. 3.2).

3.2 Methodology

The intrinsic reflectivity and specific attenuation in a common measurement domain can be retrieved by an approach using simultaneous observations by a radar network. For simplicity the setup of two anti-axially looking radars A and B is assumed, which represents a radar network along one connecting line (Fig. 3.1). $Z_{\mathrm{A},i}$ is the intrinsic

reflectivity of radar A at node i. Based on the made assumptions, within the model domain, observed by different radars A and B, the intrinsic reflectivity $Z_i = Z_{\mathrm{A},i} = Z_{\mathrm{B},i}$ and the specific attenuation $k_i = k_{\mathrm{A},i} = k_{\mathrm{B},i}$ at a common node i is considered to be equal. In this hypothetical case there are two information about the same measured quantity. As the radar forward operator is an equation with two unknowns, the retrieval method based on a linear system of equations (LSE) can be derived following Equation 3.3. The methodology's kernel is similar to a tomographic problem.

The measured reflectivities Z' of two radars A and B are mapped on the nodes of the domain $\{P_i \,:\, 1 \leq i \leq N\}$. The resulting coefficients are summarised in the observation vector

$$\vec{x}_{\mathrm{o}} = \left(Z'_{\mathrm{A},1}, ..., Z'_{\mathrm{A},N}, Z'_{\mathrm{B},1}, ..., Z'_{\mathrm{B},N}\right). \tag{3.6}$$

Similarly, the quantities to be retrieved - the intrinsic reflectivity Z and the specific attenuation k at the nodes - are stored in the unknown analysis vector

$$\vec{x_{\mathrm{a}}} = (Z_1, ..., Z_N, k_1, ..., k_N). \tag{3.7}$$

With this notation Equation 3.3 can be written as

$$\mathbf{F}\vec{x}_{\mathrm{a}} = \vec{x}_0, \tag{3.8}$$

$$\mathbf{F} = \begin{pmatrix} \mathbf{I}_N & \mathbf{B}_{\mathrm{A}} \\ \mathbf{I}_N & \mathbf{B}_{\mathrm{B}} \end{pmatrix}. \tag{3.9}$$

The forward operator matrix $\mathbf{F}$ (Eq. 3.9) consists of the identity matrices $\mathbf{I}_N$ with the dimension $N \,\mathrm{x}\, N$ and the two beam matrices $\mathbf{B}_{\mathrm{A}}$ and $\mathbf{B}_{\mathrm{B}}$ for the radars A and B, respectively. In general, $\mathbf{F}$ is large, ill-conditioned and sparse. The LSE (Eq. 3.8) is a determined equation system for two radars. Nevertheless, its solution is not trivial. The schemes are described in Section 3.3.

It is straightforward to adapt the technique to an arbitrary number of radars greater or equal two. Therefore, the LSE is expanded to a 2d-geometry and, exemplary, with three scanning radar systems A, B and C. Unlike along the connecting line, it is impossible to obtain perfectly matching range gates of the three systems, thus the beam matrices are determined independently from the radial grids of the radar systems. Standard interpolation methods, e.g. nearest neighbour, need to be applied to map the observed reflectivities to common nodes. As proceeded for the observation vector of two radars (Eq. 3.6), the resulting coefficients are summarised in the observation vector

$$\vec{x_{\mathrm{o}}} = \left(Z'_{\mathrm{A},1}, ..., Z'_{\mathrm{A},N}, Z'_{\mathrm{B},1}, ..., Z'_{\mathrm{B},N}, Z'_{\mathrm{C},1}, ..., Z'_{\mathrm{C},N}\right) \tag{3.10}$$

and the unknown analysis vector (Eq. 3.7) remains the same. The forward operator matrix $\mathbf{F}$ (Eq. 3.9) is expanded by the beam matrix $\mathbf{B}_\mathrm{C}$:

$$\mathbf{F} = \begin{pmatrix} \mathbf{I}_N & \mathbf{B}_\mathrm{A} \\ \mathbf{I}_N & \mathbf{B}_\mathrm{B} \\ \mathbf{I}_N & \mathbf{B}_\mathrm{C} \end{pmatrix}. \tag{3.11}$$

As a result, the matrix is no longer quadratic but of the dimensions $3N \,\mathrm{x}\, 2N$ with the number of nodes N. The system matrix $\mathbf{F}$ of the LSE is still sparse but huge. With the third radar, the LSE becomes over determined. Further, the equation needs to be solved by minimisation (Sec. 3.3).

3.3 Inverse Problem's Solution

The following deals with the inverse solution of the introduced forward problem. The solution of Equation 3.8 is neither for two than for more radars trivial. In general, the forward operator matrix $\mathbf{F}$ is sparse, large and partly ill-conditioned. Consequently, the LSE is not solved directly but iteratively by searching the best fitting analysis vector $\vec{x}_\mathrm{a}$ for the mathematical model $\mathbf{F}$ and the observations $\vec{x}_\mathrm{o}$, which is referred as regression. An approximate solution may found by minimising the residual vector

$$\vec{r} = \mathbf{F}\vec{x_\mathrm{a}} - \vec{x_\mathrm{o}} \tag{3.12}$$

using any well defined metric. One commonly used metric is the 2-norm of $\vec{r}$, which is called the least squares solution (Aster et al., 2013):

$$\text{minimize } \|\vec{r}\|_2 . \tag{3.13}$$

Standard minimisation schemes can be used, e.g. the LSQR scheme by Paige and Saunders (1982) or the LSMR scheme by Lim et al. (2011). The solution of inverse problems like Equation 3.13 are difficult as solution existence, solution uniqueness and instability of the solution process have to be considered (Aster et al., 2013). Although the explicit procedure of a minimisation scheme is not intended as the essential content of this thesis, conditions and possible enhancements for the solution have to discussed. For general theory of inverse problem modeling, refer to standard textbooks, e.g. Aster et al. (2013). In the following the procedure of Equation 3.3 and Equation 3.13 is referred to as the LSE-method.

As the radar forward operator (Eq. 2.2) describes the relation between the observed reflectivity Z', intrinsic reflectivity Z and path-integrated specific attenuation k, the LSE is derived by neglecting nodes without rain. These nodes are unattenuated. Using

all nodes would result in a simply wrong modelling of the system's physics. Consider the case that a weather radar observes precipitation along its observational path partially. The integration of the specific attenuation k results in a *PIA* greater zero. See Equation 2.1: $Z'(r) = Z(r) - \int_0^r k(s)\,\mathrm{d}s$. As this equation includes the *PIA* and the term is for the residual observational path greater zero, these residual reflectivities Z originally 0 dBZ are not well described. The considered case at an exemplary non-rainy node behind the precipitation area ($r = l$) is characterised by $Z(l) = 0$, $k(l) = 0$ and $Z'(l) \stackrel{!}{=} 0$. Since the integral over all k is greater than 0 dB, $Z'(l) \neq 0$. Above all, the nodes to be retrieved are reduced and thus computing capacity decreases.

This leads to the solution's challenge, that the forward operator matrix $\mathbf{F}$ is memory-intensive due to its dimension $(R \cdot N)\,\mathrm{x}\,(2 \cdot N)$, with R is the number of radars, which is greater or equal two. The number of nodes N for a grid resolution of 100 m is in the order of 10^4, thus $\mathbf{F}$ is in the order of 10^8. Assuming the entries to be 64 bit floats results approximately in memory-usage of 1 GB. The storage requirement increases for the usage of more radars. An idea to circumvent the numerical and technical difficulties of minimising the residuum for such a huge system, is a multigrid approach as used in mathematics. The model is solved iteratively on a very coarse grid. The grid is successively refined and the coarser scale solution is used every time as first guess for the minimisation at the next level. Since attenuation is an integral effect, it is reasonable to assume that this approach increases the convergence speed on the minimisation significantly. Refer to Xu and Zikatanov (2017) for details on standard multigrid approaches.

Another possibility to improve the solution scheme is to apply other regressions. The $L1$ regression is the 1-norm of the $\vec{r}$ and could be beneficial because least squares solutions are highly sensible to outliers, which may arise from measurement errors. Nevertheless, $L2$ regression with the 2-norm is used because the least squares solution is unbiased in statistical terms (Aster et al., 2013).

Furthermore, the inverse solution can be highly unstable in that small changes of observations, like noise, can lead to an erroneous change in the estimation. This LSE is said to be ill-conditioned. Additional constraints can stabilise the solution. Information, like the knowledge that the specific attenuation is always greater or equal zero, can be added with the method of Lagrange multipliers. The method of Tikhonov regularization can be used for stabilising inverse problem solutions in common, where a damped and constrained minimisation is considered (Aster et al., 2013).

However, regularisation or more complex schemes are beyond the scope of this work. This thesis aims to show fundamental opportunities of the LSE-method. Thus, the retrieval method is explored with a basic LSE (Chap. 4).

4 Experimentation of the Retrieval Algorithm on Synthetic Radar Data

The following chapter covers the implementation of the retrieval method for attenuation and reflectivity in a networked environment, as proposed in Chapter 3. In order to apply the retrieval algorithm an evaluation is required. For that reason, a sensitivity analysis is realised by implementing the retrieval algorithm on weather radar data with a superimposed varying uncertainty. To have simultaneous weather radar observations with and without the impact of attenuation and uncertainty, synthetic data is generated. The first step of this process is to consider an idealised box precipitation in an one-dimensional weather radar network's setup along the connecting line (Fig. 3.1). Step by step the setup's complexity is enhanced. The precipitation varies from constant boxes to fluctuating fields based on Gaussian random fields. The model's geometry enlarges from one to two dimensions. The weather radar network expands from two to three radars. The conceivable error sources are introduced separately. All in all, realistic weather radar observations are approximated and isolated effects on the retrieval's solution are investigated. Details on evaluation's methodology are summarised in Section 4.1. The synthetic weather radar data with its different complexity is described in Section 4.2. The synthetic data is investigated for several setups: a constant one-, two-dimensional field, and a realistically structured two-dimensional Gaussian field in Section 4.3.

Note, as there are different outputs for same variables one notation is defined. Consider a quantity x. The observation of this quantity is indicated by a prime: x'. The retrieved quantity is indicated by a hat: $\hat{x}$. The intrinsic quantity is just as it is: x. Quantity x is in fact the vector $\vec{x}$ and includes more than one entry for each node. In the following this notation is used.

4.1 Methodology

The structure of the evaluation's procedure of the LSE-method is summarised in an outline similar to a flowchart (Fig. 4.1). The first step is to consider an intrinsic reflectivity Z and specific attenuation k. Isolated uncertainties, e.g. noise or local perturbations, can superimpose these given quantities. Noise and clutter is known to be additive to

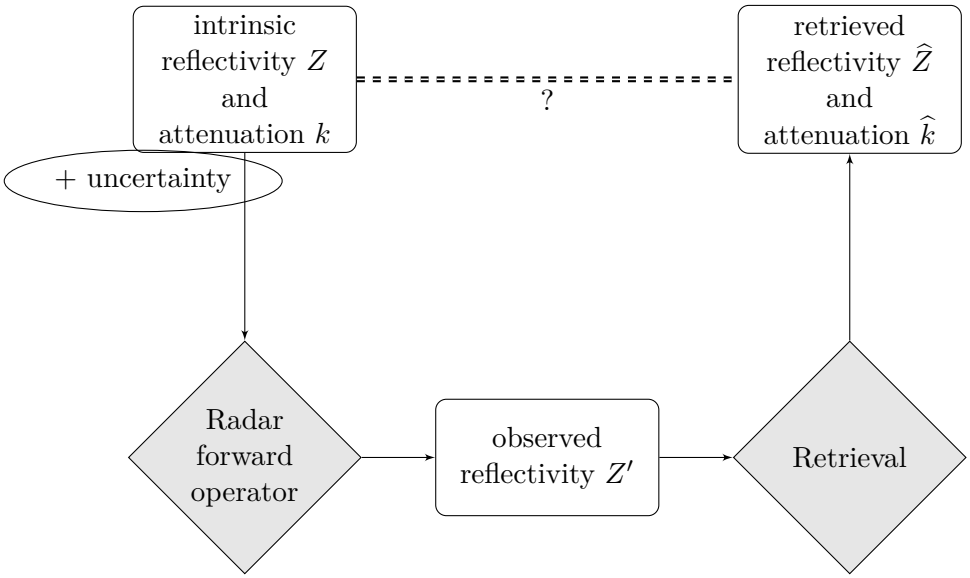

Figure 4.1: Outline for evaluating the retrieval method using synthetic data.

the measurements (Doviak and Zrnić, 1993). The intrinsic reflectivity Z and specific attenuation k are transferred to the observed reflectivity Z' by using a radar forward operator (Eq. 2.2). The discretised radar forward operator is introduced in Section 3.1. The retrieval method is applied on this synthetic observed reflectivity Z', as the LSE-method is the inverse solution of the radar forward operator. Thus, the application of the method results in the retrieved reflectivity $\hat{Z}$ and specific attenuation $\hat{k}$. The expectation is that the retrieved and intrinsic reflectivity and attenuation are equal: $\hat{Z} \stackrel{!}{=} Z$ and $\hat{k} \stackrel{!}{=} k$. The comparison of the retrieval with the truth examining several setups is used as evaluation. Every uncertainty is added isolated, thus it can be determined how sensible the LSE-method reacts. The sensibility between the uncertainty effects can be compared using established measures. These measures - bias and root-mean-square error (RMSE) - are used as defined in the following:

$$\mathrm{BIAS}(\widehat{x}) = \frac{1}{N}\sum_{i=1}^{N} \widehat{x}_i - x_i, \tag{4.1}$$

and

$$\mathrm{RMSE}(\widehat{x}) = \sqrt{\frac{1}{N}\sum_{i=1}^{N} (\widehat{x}_i - x_i)^2}, \tag{4.2}$$

with N is the number of nodes, x is the intrinsic, and $\widehat{x}$ is the retrieved quantity.

Note, there are two synthetic precipitation origins. The intrinsic quantities can be given in Cartesian or polar radar coordinates, as measured. If the reflectivity is given in polar radar coordinates, the attenuation can be subtracted range bin to range bin over the propagation path to apply the forward operation. In that case the observations have

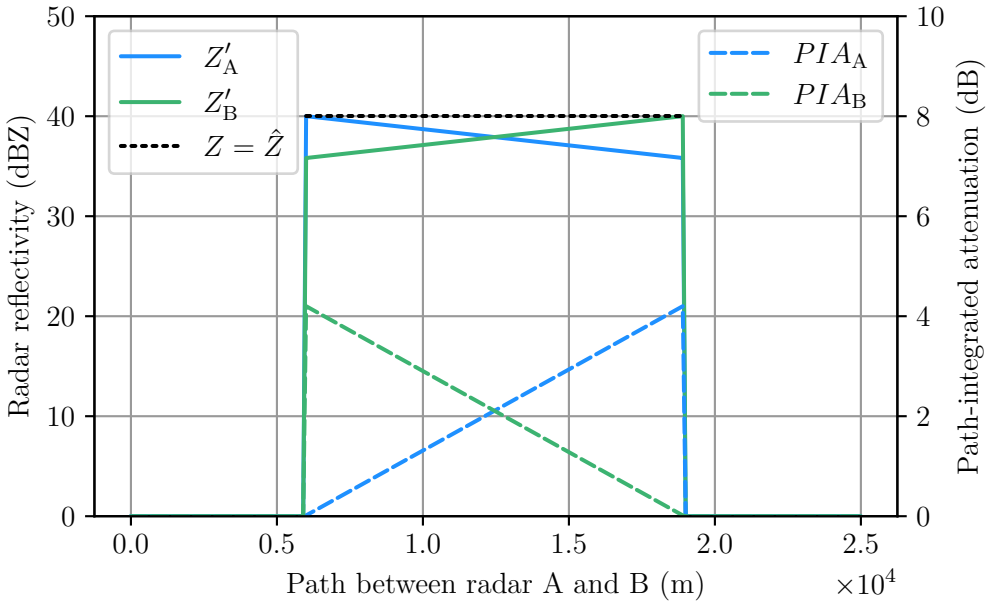

Figure 4.2: Synthetic one-dimensional box precipitation in quantities of radar reflectivity Z and path-integrated attenuation (PIA). Observations are indicated by a prime ($'$), retrieved quantities are indicated by a hat ($\hat{}$) and intrinsic quantities have no special indication.

to be interpolated onto a Cartesian grid to apply the proposed LSE-method. Since the interpolation might be another element of uncertainty, most cases are set in Cartesian coordinates so that the focus is on the retrieval method. The synthetic precipitation areas mapped on the coordinates is described in Section 4.2.

4.2 Data

The synthetic weather radar data is the basis of the retrieval's evaluation because the truth of the retrieved quantities is known.

One-dimensional box precipitation

The first step towards the application of the LSE-method on real data is to explore the algorithm in simple manner. A synthetic one-dimensional box precipitation observed by two radars (radar A and radar B) along the connecting line is considered (Fig. 4.2). The radars observe a constant precipitation area characterised by a rain rate R of $10\,\mathrm{mm\,h^{-1}}$ and an expanse of 12900 m. The model domain covers 25000 m discretised on 2500 nodes. With appropriate relations, the rain rate R can be transferred to the intrinsic reflectivity Z and specific attenuation k. For this purpose an exemplary z-R-relation

$$z = 400 \cdot R^{1.4} \tag{4.3}$$

and k-R-relation

$$k = 0.01 \cdot R^{1.21} \tag{4.4}$$

are used, where Z is the intrinsic reflectivity in $\mathrm{mm}^6\,\mathrm{m}^{-3}$, k is the intrinsic specific attenuation in $\mathrm{dB\,km}^{-1}$, and R is the rain rate in $\mathrm{mm\,h}^{-1}$ (Doviak and Zrnić, 1993). According to Equation 4.3 and Equation 4.4 the box precipitation results in radar quantities of $Z = 40.02\,\mathrm{dBZ}$ and $k = 0.16\,\mathrm{dB\,km}^{-1}$. The radar forward operator (Sec. 3.1) results in the observed reflectivities Z'_A and Z'_B decreasing linearly to 35.82 dBZ (Fig. 4.2). The path integral of the specific attenuation k integrated over the full path,

$$PIA = \int k\,\mathrm{d}s, \tag{4.5}$$

results in $PIA_\mathrm{A} = PIA_\mathrm{B} = 4.20\,\mathrm{dB}$ influencing the observations of both radars.

Two-dimensional box precipitation

To enhance complexity of the scenario for the retrieval's evaluation, the one-dimensional setup is expanded to a two-dimensional geometry (Fig. 4.3). The domain covers $25000\,\mathrm{m} \times 22000\,\mathrm{m}$ discretised on 598 nodes. The values are considered to be the same as in the one-dimensional case with $R = 10\,\mathrm{mm\,h}^{-1}$, $Z = 40.02\,\mathrm{dBZ}$ and $k = 0.16\,\mathrm{dB\,km}^{-1}$. The two-dimensional geometry makes it possible to place two, three (Fig. 4.3) or more radars inside the model domain. The radar forward operator (Sec. 3.1) results in the observed reflectivity and attenuation. According to Equation 4.5 the observations of three radars A, B and C are influenced up to a maximum of $PIA_\mathrm{A} = 8.86\,\mathrm{dB}$, $PIA_\mathrm{B} = 8.86\,\mathrm{dB}$ and $PIA_\mathrm{C} = 8.29\,\mathrm{dB}$. The radar reflectivity and specific attenuation can be retrieved on the basis of either two or three observations, thus the LSE is either determined or over determined. However, constant observations are still oversimplifying the problem.

Two-dimensional Gaussian field

A realistically structured synthetic two-dimensional precipitation area is created for the evaluation (Fig. 4.4). For this purpose, the radar reflectivity is assumed to be of Gaussian random fields (Abrahamsen, 1997; Powell et al., 2014). Details on Gaussian random fields exceed the scope of this thesis, therefore refer to Abrahamsen (1997). The method uses the assumption that a reflectivity field Z in the limits of 0 dBZ and 70 dBZ is created (Fig. 4.4a). The intrinsic specific attenuation is derived with Equation 4.3 and Equation 4.4 (Fig. 4.4b). This exemplary, intrinsic radar reflectivity is in the limits of 0.00 dBZ and 62.92 dBZ. The associated, intrinsic specific attenuation is in the limits of $0\,\mathrm{dB\,km}^{-1}$ and $9.44\,\mathrm{dB\,km}^{-1}$. According to the radar forward operator (Eq. 3.1) the

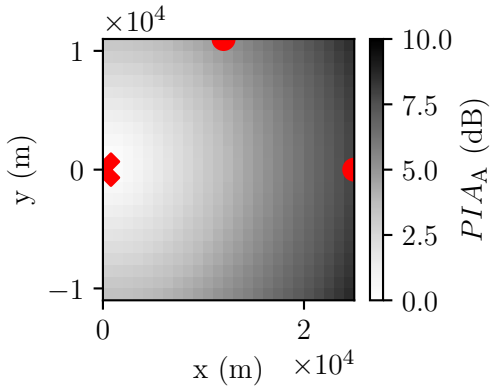

(a) Radar A.

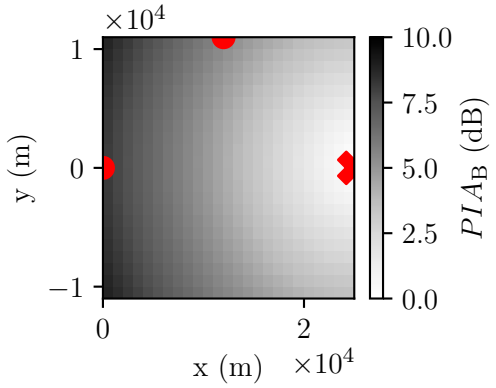

(b) Radar B.

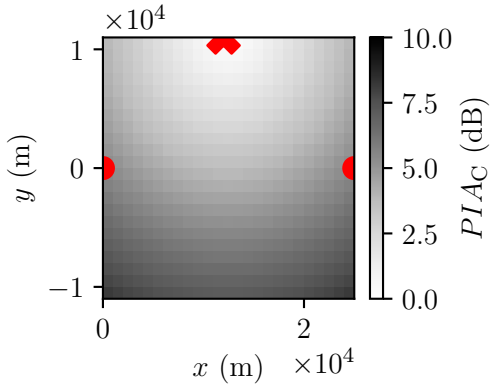

(c) Radar C.

Figure 4.3: Synthetic two-dimensional box precipitation in quantities of *PIA* covering the area of exemplary radars. The radar sites are indicated by red markers. The regarding radar site is indicated by a cross.

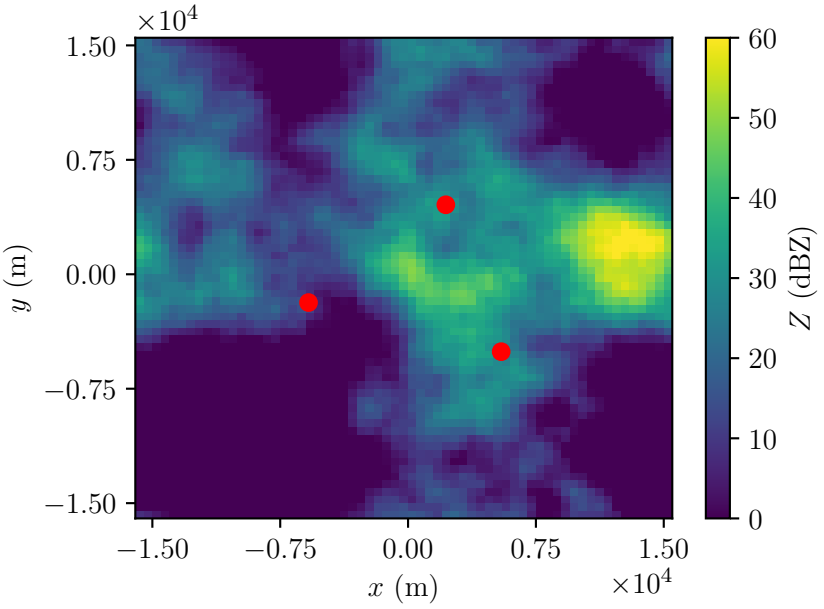

(a) Reflectivity.

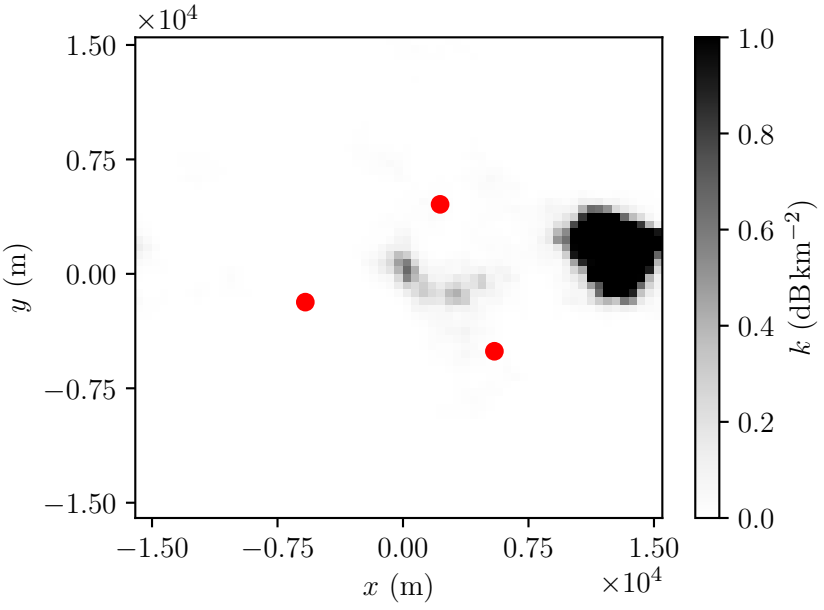

(b) Specific attenuation.

Figure 4.4: Synthetic two-dimensional precipitation in quantities of radar reflectivity and specific attenuation covering PATTERN-area. The red dots indicate the radar sites HWT (north), MOD (east), BKM (west).

observed reflectivity Z' is in the limits of $-25.49\,\mathrm{dBZ}$ and $53.57\,\mathrm{dBZ}$. The *PIA* influences up to a maximum of $55.99\,\mathrm{dB}$ following Equation 4.5. Although the considered values are overstated, this test case is suitable as an object of investigation because of the structure of the field. The synthetic two-dimensional model domain covers the PATTERN-area with 32000 m x 32000 m discretised on 4096 nodes, which corresponds to a 500 m resolution. In general, the retrieval's application on this synthetic field can demonstrate the capability of the LSE-method on realistic structures.

The evaluation of the retrieval is discussed for these three theoretical setups. The intrinsic observations fulfil the assumptions as defined for the LSE-method, see Chapter 3:

- The observations are vertically homogeneous.
- The intrinsic reflectivity is equal for same nodes.
- The measurements are simultaneous.

4.3 Retrievals

The LSE-method is evaluated for synthetic, two-dimensional, and realistic structured precipitation areas. Initially, the retrieval of idealised box precipitation is evaluated in one dimension and in two dimensions.

One-dimensional constant field retrieval

The LSE-method is applied to the synthetic one-dimensional box precipitation observed by two radars along the connecting line (Sec. 4.2). The intrinsic data has no uncertainty in form of noise or local perturbations. Following the outline for the evaluation (Fig. 4.1), the retrieval algorithm results in the expectations. The intrinsic and retrieved quantities are equal (Fig. 4.2). Changing the expansion of the one-dimensional box precipitation including 2500 nodes to a an uneven number, e.g. 2501 nodes, leads to a singular LSE. The singular solution of the LSE is challenging and requires regularisation procedures. Refer to Aster et al. (2013) for advanced solving methods. Notwithstanding the singular case, the simple retrieval method with its non-singular LSE is investigated for further setups. Additional uncertainties are examined for the one-dimensional constant field retrieval.

As clutter influences the radar signal locally (Lengfeld et al., 2014), these perturbations may have an impact on the performance of the retrieval technique. Following the evaluation's outline (Fig. 4.1), local perturbations are considered to superimpose the synthetic observations. The perturbations are at different locations for both radar observations (Fig. 4.5). Radar A measures the reflectivity Z'_{A} at 9.9 km and 10.1 km

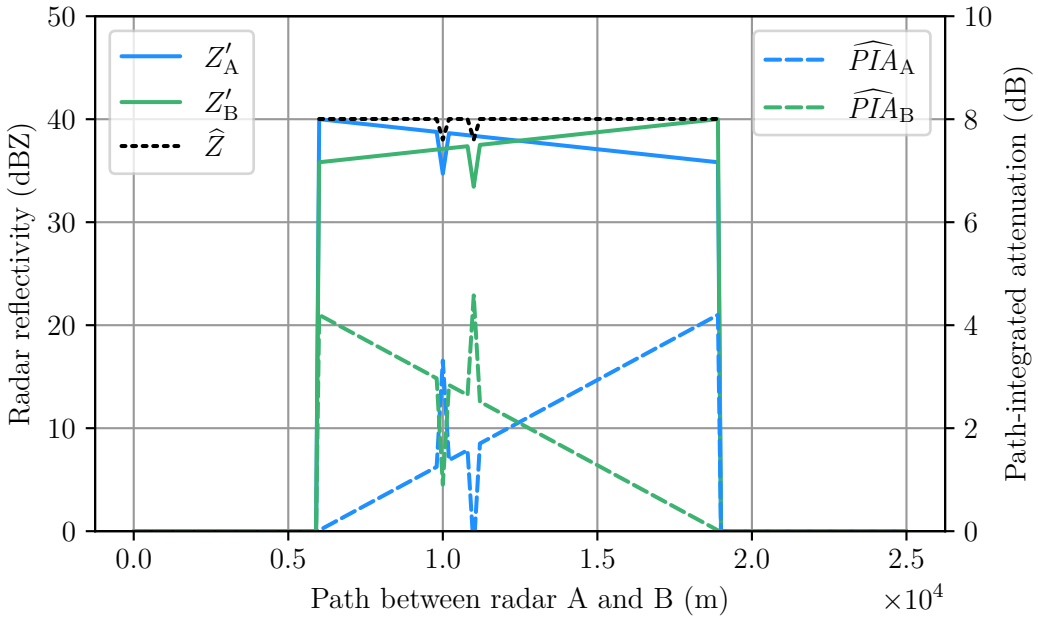

Figure 4.5: Retrieval on synthetic one-dimensional box precipitation in quantities of radar reflectivity and path-integrated attenuation with superimposed local perturbations on the observations. Analogous visualisation to Figure 4.2.

with $-2\,\mathrm{dB}$ and at 10.0 km with $-4\,\mathrm{dB}$ offset. Analogously, radar B observes the equal differences in Z'_{B} at 10.8 km, 10.9 km and 11.0 km. The perturbations have impact on the results of the LSE-method. The retrieved reflectivity $\widehat{Z}$ is nearly negligible negative biased as the perturbation introduces negative differences: $\mathrm{BIAS}(\widehat{Z}) = -0.06\,\mathrm{dB}$. Generally, the impact of local perturbations on $\widehat{Z}$ remain at the perturbations' locations. As a result, the RMSE is driven by the standard deviation: $\mathrm{RMSE}(\widehat{Z}) = 0.30\,\mathrm{dB}$. The retrieved specific attenuation $\widehat{k}$ is not biased. Nevertheless, the local perturbations influence $\widehat{k}$. The retrieved specific attenuation $\widehat{k}$ is characterised by significant local overestimation and underestimation: $\mathrm{RMSE}(\widehat{k}) = 1.75\,\mathrm{dB\,km^{-1}}$. The resulted RMSE is one magnitude greater than the intrinsic specific attenuation $k = 0.16\,\mathrm{dB\,km^{-1}}$. The effect of the local perturbations on $\widehat{k}$ is shown in the form of the *PIA* in Figure 4.5. The solution becomes locally unstable. There are negative results in $\widehat{k}$, which are not physically plausible but mathematically possible. For the case that the local perturbations are considered to be at the same locations the retrieval algorithm results in the expected solution: $Z = 40.02\,\mathrm{dBZ}$ and $k = 0.16\,\mathrm{dB\,km^{-1}}$. The retrieved reflectivity $\widehat{Z}$ preserve the local negative perturbation. The retrieved specific attenuation $\widehat{k}$ results in the exact constant value. In summary, local perturbations impact the solution of the LSE-method locally.

Note, that ideally the radar data's preprocessing removes clutter and interpolates missing data. But, remaining missing values have an impact on the solution of the

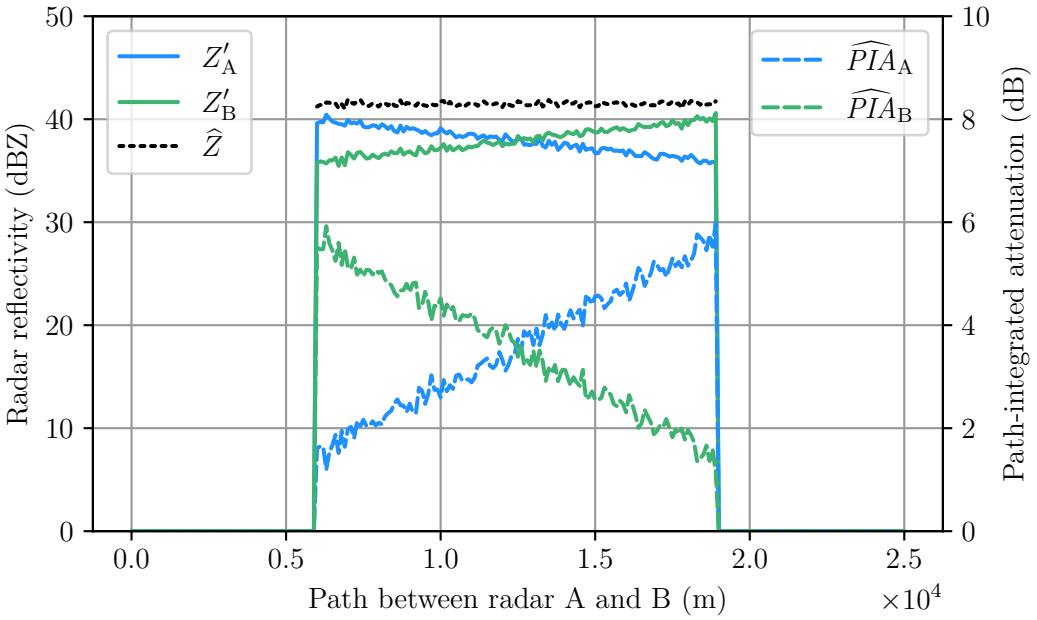

Figure 4.6: Retrieval on synthetic one-dimensional box precipitation in quantities of radar reflectivity and path-integrated attenuation with superimposed Gaussian noise sample (STDEV(n) = 0.25 dB) on the observations. Analogous visualisation to Figure 4.2.

retrieval. The LSE-method includes only nodes with existing observations of all respective radars. Therefore, missing values within the LSE lead to the underestimation of *PIA* affecting the retrieval's solution.

Additionally to clutter, the radar measurements are affected by noise induced by the atmosphere and internal electronics. The noise is generally removed by existing algorithms (Lengfeld et al., 2014). Nevertheless, the possible impact of remaining noise on the performance of the retrieval technique needs attention. Some noise can remain in the measurements. Following the evaluation's outline (Fig. 4.1), Gaussian random noise samples are considered to superimpose the synthetic observations (Fig. 4.6). The noise n as random noise sample from a normal distribution has the standard deviation STDEV(n). The noise is radar-dependent. Therefore, different noise samples with the same STDEV are created. In the event the noise samples superimpose the synthetic radar reflectivities Z'_{A} and Z'_{B} with STDEV(n) = 0.25 dB (Fig. 4.6), the LSE-method results in a biased reflectivity $\widehat{Z}$ and attenuation $\widehat{k}$: BIAS($\widehat{Z}$) = 1.46 dB and BIAS($\widehat{k}$) = 0.11 dB km^{-1}. These noisy observations do not result in a noisy retrieved reflectivity $\widehat{Z}$ (Fig. 4.6). Consequently, the RMSE of the retrieved reflectivity $\widehat{Z}$ is primarily driven by the bias: RMSE($\widehat{Z}$) = 1.47 dB. The RMSE of the retrieved attenuation $\widehat{k}$ is dominated by noise and thus the standard deviation: RMSE($\widehat{k}$) = 20.40 dB km^{-1}. With this RMSE the attenuation retrieval is random. Nevertheless, the unusable result

is reasonable as the STDEV of the noise is 10 times greater than the magnitude of the smallest quantity to retrieve, which is the specific attenuation. The specific attenuation with its constant value of $0.16\,\mathrm{dB\,km^{-1}}$ is retrieved for every node on the grid with a resolution of 100 m. Thus, the quantity to retrieve is $0.016\,\mathrm{dB\,node^{-1}}$ but with this superimposed noise the information is lost. To quantify the effect of noise, an ensemble of retrievals with different noise samples n is examined (Fig. 4.7). A number of 10000 ensembles is considered. The standard deviation of the superimposed noise samples STDEV(n) is limited up to roughly 1 dB. In detail the range of STDEV(n) is subdivided in 100 values and for every value 100 noise samples are generated, so the ensemble members are evenly distributed. One outcome of the ensemble study is that with increasing STDEV(n) the retrieval's uncertainty grows respectively. Different noise samples with same STDEV(n) can result in entirely different results (Fig. 4.7). The retrieved radar reflectivity is appropriate in some cases but the number of ensembles with strong bias and RMSE increases with increasing STDEV(n) (Fig. 4.7a). The retrieval's solution for the specific attenuation becomes random with increasing STDEV(n) as the RMSE is mainly driven by the standard deviation (Fig. 4.7b). All in all, the retrievals characterised by strong bias and RMSE occur for a standard deviation of the noise sample STDEV(n) greater than 10 times of the magnitude of the specific attenuation per node: $> 10 \cdot \mathrm{O(k)}$. The information of this quantity is lost in significant noise. For moderate noise ($< 10 \cdot \mathrm{O(k)}$) the retrieval's solution is reliable based on the measures of bias and RMSE. This moderate noise is expected since it is removed within the processing chain of the radar data (Chap. 5). The noise is assumed to be negligible for rain events compared to non- or light rain events. Additionally, the attenuation correction with the LSE-method is needed for rain events, especially strong ones. In summary, the expected noise results in an robust solution of the LSE-method. As Chapter 5 deals with real radar data, the range of noise values is shown.

Note, the uncertainties are added in logarithmic unit even though they are only additive in linear unit. However, the usage of logarithmic unit is more clearly and the impact of uncertainties on the retrieval algorithm remains the same. As the impact of local perturbations and noise on the retrieval's solution is known, the complexity of the setup is enhanced by a retrieval for two-dimensional constant fields.

Two-dimensional constant field retrieval

The LSE-method is applied to the two-dimensional box precipitation (Sec. 4.2). As a first step, the observations of two radars are used to retrieve the constant reflectivity and specific attenuation describing the box precipitation (Fig. 4.8). The observed reflectivity is not superimposed by uncertainties. Following the evaluation's outline (Fig. 4.1), the LSE-method results in the expectations, similar to the simple, one-

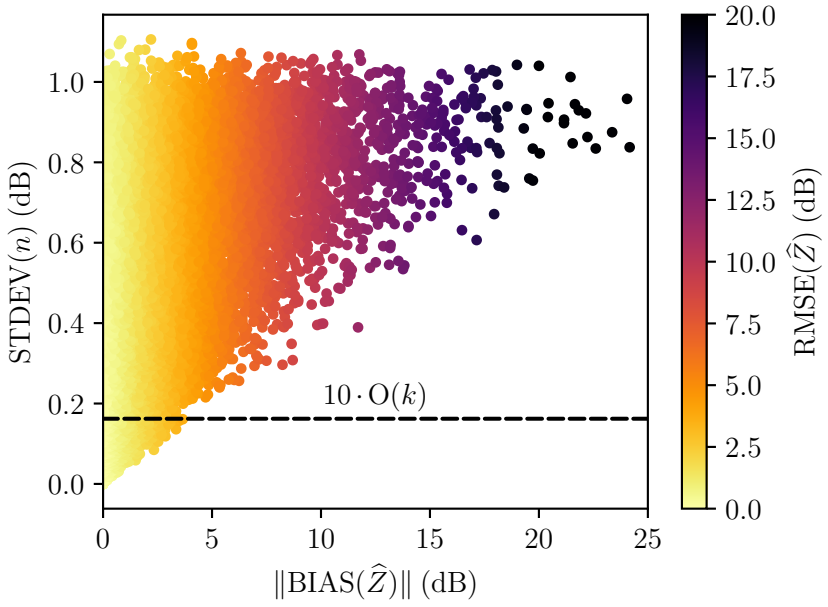

(a) Radar reflectivity $\widehat{Z}$.

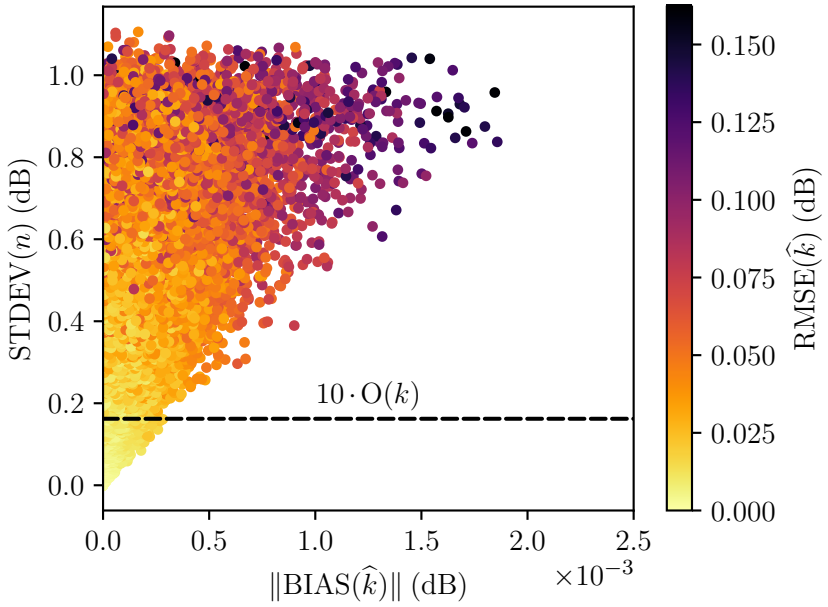

(b) Specific attenuation $\widehat{k}$.

Figure 4.7: Retrieval on synthetic one-dimensional box precipitation. Gaussian noise samples n with different standard deviations STDEV superimpose the observed reflectivities. The horizontal line shows ten times the smallest quantity to retrieve, the intrinsic specific attenuation k respective to the spacial resolution. The bias and RMSE of the quantities measure the impact of noise on the retrieval's solution.

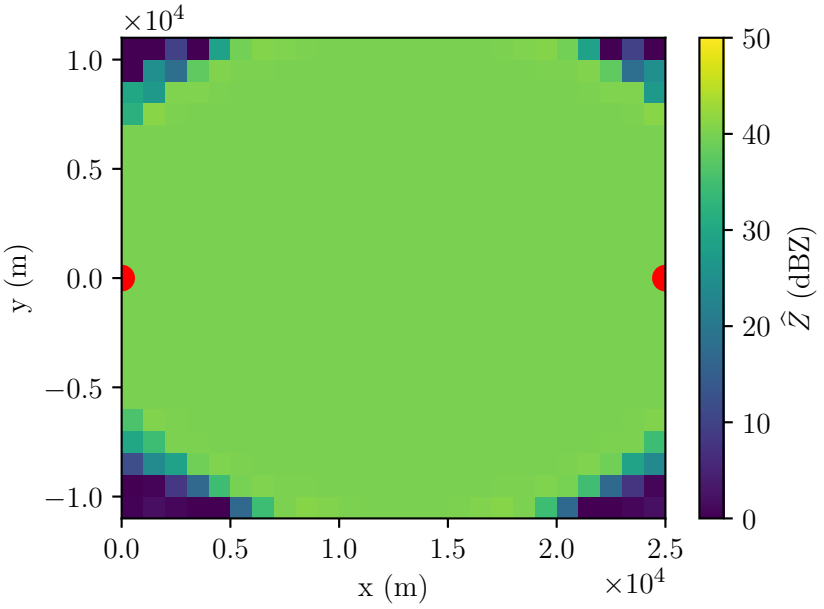

(a) Reflectivity.

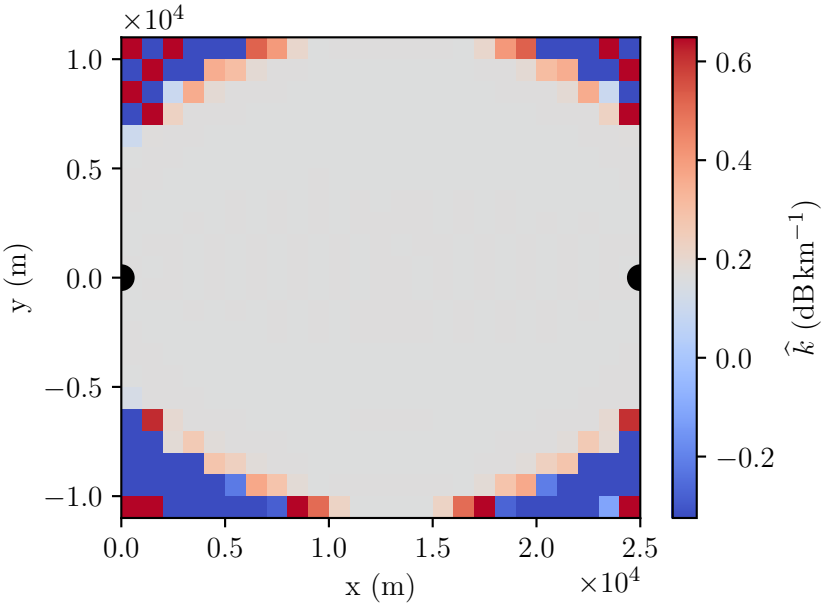

(b) Specific attenuation.

Figure 4.8: Reflectivity and attenuation retrieved from a two-dimensional constant field observed by two radars. The dots indicate the two radar sites A (west) and B (east).

dimensional solution, but only partially. The quality of the result decreases at the edges of the model domain. In the domain's centre the intrinsic and retrieved reflectivity and specific attenuation are equal (Fig. 4.8). Nevertheless, the radar reflectivity $\widehat{Z}$ is biased with $-3.48\,\mathrm{dB}$ and has a RMSE of $11.83\,\mathrm{dB}$. The retrieved specific attenuation $\widehat{k}$ is negative biased with $-0.94\,\mathrm{dB\,km^{-1}}$ and is characterised by a RMSE of $6.60\,\mathrm{dB\,km^{-1}}$. The measures correspond to the incorrect results at the edges. One assumption for this uncertainty is that the retrieval's solution tends to instability because less equations of the LSE have an impact on the results of the edge nodes. The difficulty of the singular solution, as described in one dimension, maintains in this setup. For that reason, an uneven number of nodes between two radar sites is a challenge. However, the observations by a third radar (Fig. 4.3) stabilise the solution of the LSE-method. With three or more radars the LSE is overdetermined. The probability of a singular LSE is minimised. Additionally, the quality of the result increases at the edges of the model domain. For this setup (Fig. 4.8), the intrinsic and retrieved radar reflectivity $\widehat{Z}$ and specific attenuation $\widehat{k}$ are equal. In summary, increasing the number of independent information, e.g. by further radar observations, stabilises the solution of the LSE-method. In the following, additional uncertainties are examined for the two-dimensional constant field retrieval. The results of the one-dimensional retrieval are straightforward applicable to two dimensions.

Beside clutter and noise, the networked weather radar observations may be biased due to different calibrations (Lengfeld et al., 2014). Ideally, an absolute calibration based on MRR measurements (Lengfeld et al., 2014) or at least relative calibration (Burgemeister, 2018) is applied. Nonetheless, the impact of biased radar observations on the retrieval's solution is considered (Fig. 4.9 and 4.10). The setup is still the two-dimensional constant field observed by the three radars A, B and C. The exemplary calibration errors c, superimposing the observations, are for radar A $c_\mathrm{A} = 2\,\mathrm{dB}$, radar B $c_\mathrm{B} = -3\,\mathrm{dB}$ and Radar C $c_\mathrm{C} = 0\,\mathrm{dB}$. The calibration errors result in an appropriate retrieval for the radar reflectivity $\widehat{Z}$: $\mathrm{BIAS}(\widehat{Z}) = 0.04\,\mathrm{dB}$ and $\mathrm{RMSE}(\widehat{Z}) = 1.00\,\mathrm{dB}$ (Fig. 4.9a). Some outliers are located at the edge of the model domain. Although the retrieved specific attenuation $\widehat{k}$ has no bias, the values vary widely: $\mathrm{RMSE}(\widehat{k}) = 0.88\,\mathrm{dB\,km^{-1}}$ (Fig. 4.9b). With this variation of the specific attenuation $\widehat{k}$, the retrieval is not reliable. To quantify the calibration's impact on the solution of the LSE-method, an ensemble study with this setup is performed (Fig. 4.10), analogous to the noise ensemble study in one dimension (Fig. 4.7). A number of 1000 ensembles is considered. Calibration biases c are added to the observed reflectivities Z'. The calibration biases are similar to real parameters worked out by Lengfeld et al. (2014). The absolute sum of the three calibration biases c measures the total calibration bias. On the one hand, the retrieval of the radar reflectivity $\widehat{Z}$ is robust against the calibration error

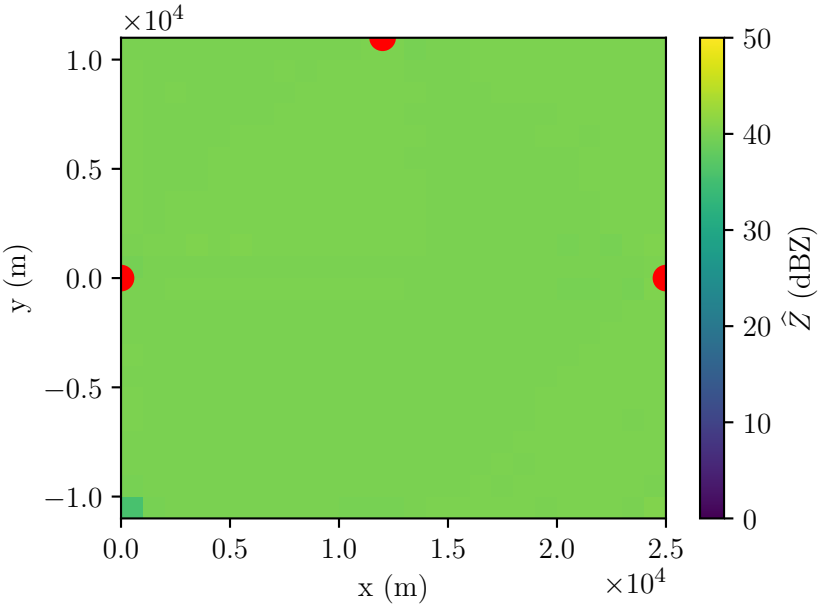

(a) Reflectivity.

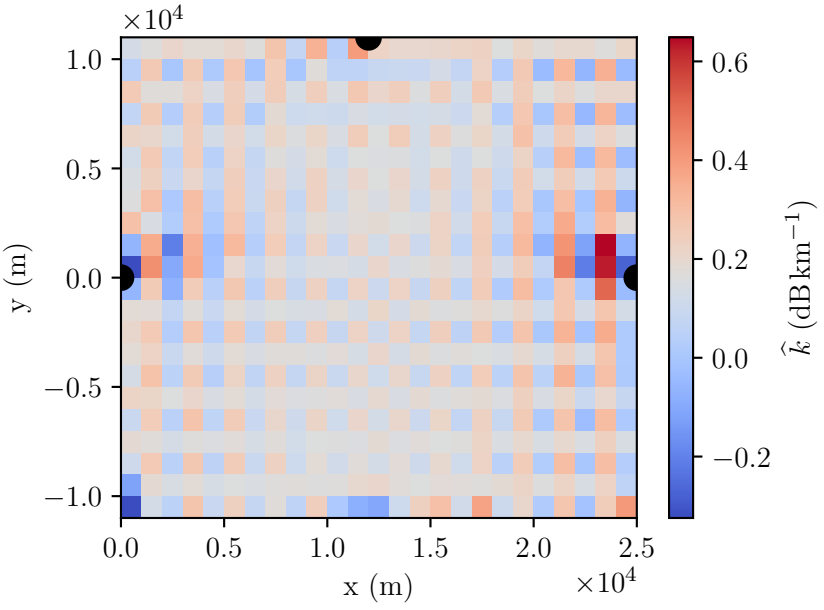

(b) Specific attenuation.

Figure 4.9: Reflectivity and attenuation retrieved from a two-dimensional constant field observed by three radars biased by a calibration error. The dots indicate the three radar sites A (west), B (east), C (north).

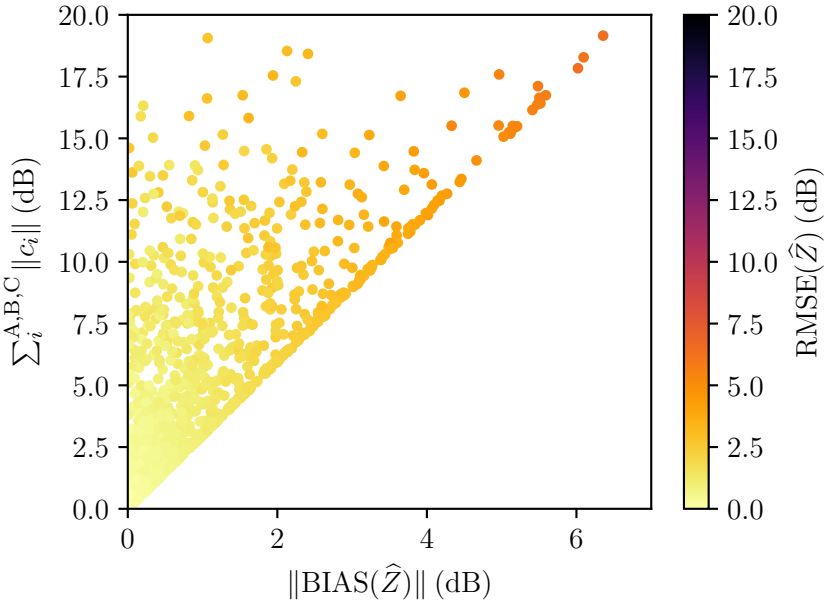

(a) Radar reflectivity $\widehat{Z}$.

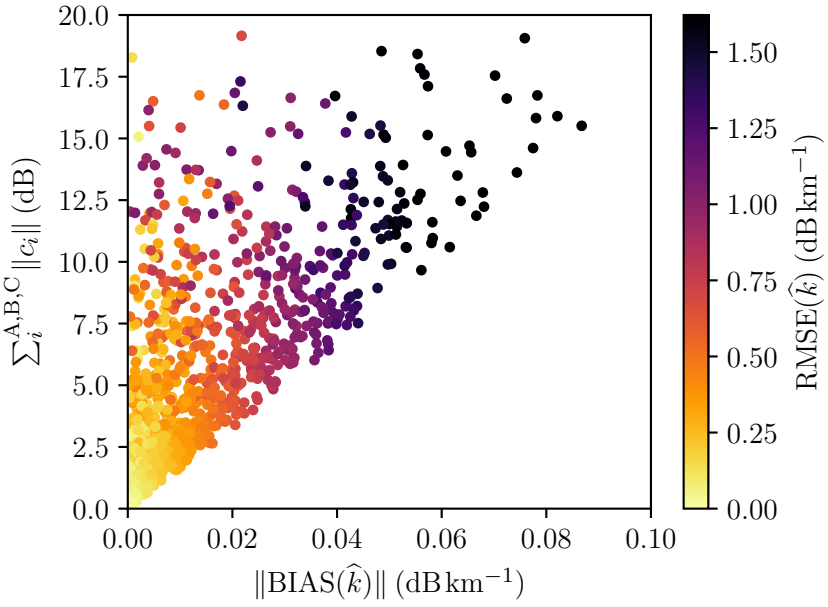

(b) Specific attenuation $\widehat{k}$.

Figure 4.10: Retrieval on synthetic two-dimensional box precipitation. Calibration biases c superimpose the observed reflectivities Z' of the three radars A, B and C. The bias and RMSE of the quantities measure the impact of the calibration bias on the retrieval's solution.

because the bias and RMSE are relative small compared to the intrinsic reflectivity Z (Fig. 4.10a). On the other hand, a total calibration bias results in fluctuating retrieved specific attenuations $\widehat{k}$ as shown with the RMSE (Fig. 4.10b). The bias of the specficic attenuation $\widehat{k}$ is small compared to the intrinsic specific attenuation $k = 0.16\,\mathrm{dB\,km^{-1}}$. In summary, a well-calibrated weather radar network is mandatory for the application of the LSE-method.

Further to clutter, missing values, noise, and calibration errors, the used interpolation method may introduce uncertainty. Based on the outline for the evaluation of the retrieval method (Fig. 4.1), the two-dimensional constant field is discretised on the polar observation grids of the three radars A, B and C. The considered polar observation grid is characterised by 1° azimuth resolution in a range between 0° and 359° and a distance resolution of 1000 m in a range between 0 m and 27000 m. The intrinsic specific attenuation is subtracted for each range bin and azimuth over the propagation path to infer the forward operation. The attenuated observations of the three radars are interpolated on the Cartesian two-dimensional model domain (Fig. 4.4) by an arbitrary linear interpolation method. Applying the LSE-method to the simple solution results in the expectations: the intrinsic and retrieved quantities are equal. Nevertheless, an ill-suited interpolation method manipulating the data introduces uncertainty because the modified observations would not apply to the basis of the LSE-method.

The impact of local perturbations, missing values, noise, calibration errors and number of observation on the retrieval's solution is known for one- and two-dimensional constant field retrievals. Each error source creates difficulties so that with a certain disturbance the LSE becomes instable, which hinders a solution of the retrieval. Due to the magnitude of the different quantities, the retrieval of the radar reflectivity $\widehat{Z}$ is more stable than of the specific attenuation $\widehat{k}$. Because the assumption of a constant field of radar reflectivity and specific attenuation oversimplifies the complexity, a two-dimensional Gaussian field retrieval is investigated.

Two-dimensional Gaussian field retrieval

The LSE-method is applied to a realistic structured two-dimensional precipitation area based on Gaussian random fields (Sec. 4.2). It should be noted that the findings based on the retrieval analysis of the box-precipitation are straightforward applicable to the realistic structured precipitation. In this setting, the theoretical precipitation area covers the PATTERN-area (Sec. 2.1) and is observed by the three weather radars HWT, MOD and BKM. The observation of intrinsic reflectivity by the respective radars is distinct due to the different integrated attenuation along the paths, the *PIA* (Fig. 4.11). Applying the LSE-method to these undisturbed observed reflectivities Z' results in the expectations. The intrinsic and retrieved quantities are equal: $Z = \widehat{Z}$ and

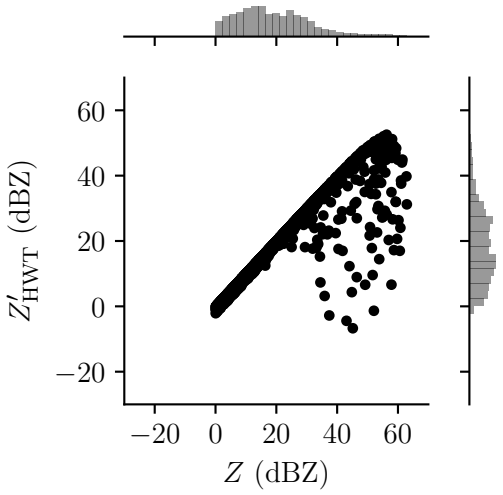

(a) Radar HWT.

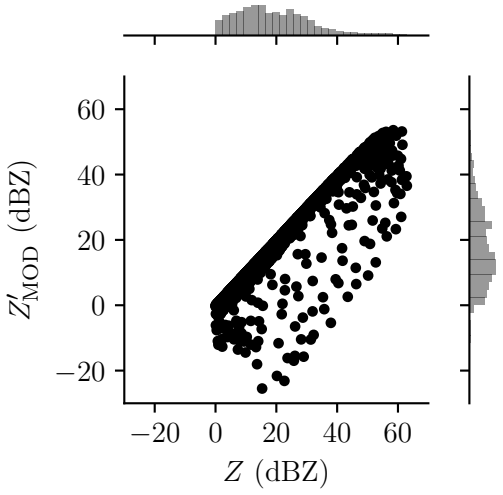

(b) Radar MOD.

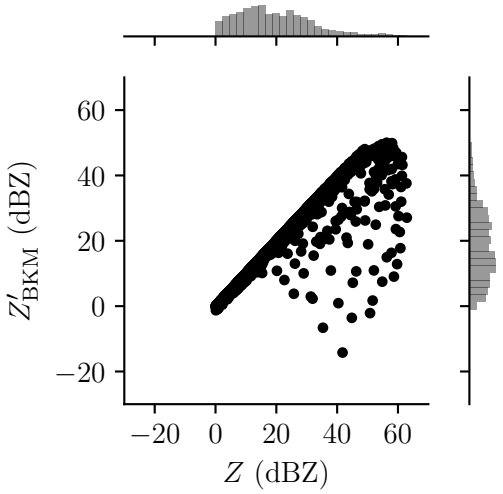

(c) Radar BKM.

Figure 4.11: Distribution between the observed and intrinsic radar reflectivity of a two-dimensional precipitation area based on Gaussian random fields.

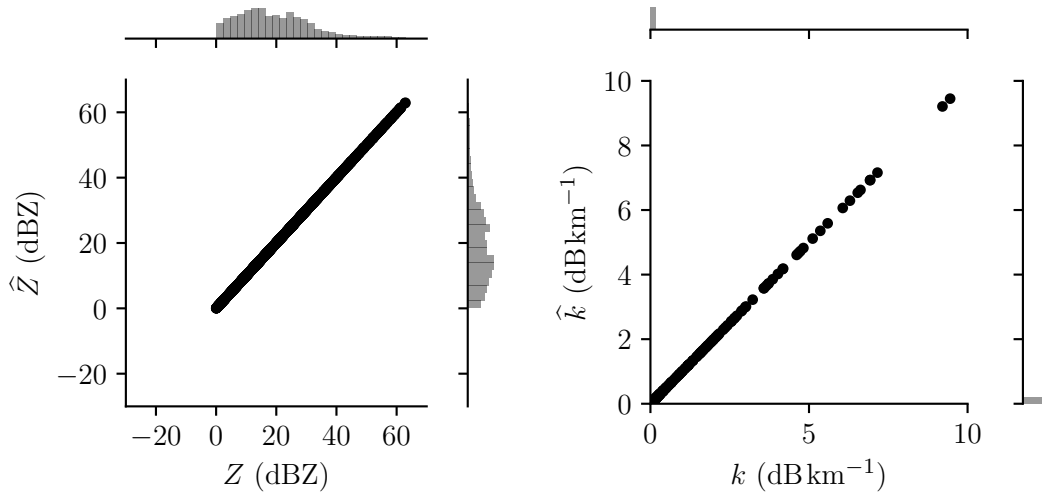

(a) Radar reflectivity.

(b) Specific attenuation.

Figure 4.12: Distribution between the retrieved and intrinsic quantities of a two-dimensional precipitation area based on Gaussian random fields.

$k = \widehat{k}$ (Fig. 4.12). The LSE-method is applicable to realistic structured precipitation taking the presumptions into consideration, described in Section 4.2.

On the contrary, the value range of the damped observed reflectivities consist of values below 0 dBZ (Fig. 4.11). Reflectivities $Z < 0\,\mathrm{dBZ}$ are no rain events. A reflectivity Z of 10 dBZ is in terms of a rain rate R smaller than $0.1\,\mathrm{mm\,h^{-1}}$ according to Equation 4.3. The specific attenuation k is negligible for this value range. Within an implementation of the LSE-method on real weather radar data, these small observed reflectivities need to be discarded because of the insufficient measurement's sensitivity. As a result, depending on the precipitation pattern, also relevant reflectivity values may be discarded. Intrinsic reflectivities Z greater than 10 dBZ are relevant. Otherwise, the algorithm could create artificial rain events. Missing relevant values lead to an underestimation of *PIA*, as described in one dimension. In summary, patterns with strong attenuation lose information because observed reflectivities get lost in measurement's sensitivity. The LSE-method is applicable to realistic structured precipitation with limitations of every attenuation correction.

All in all, the experimentation of the LSE-method on synthetic radar data demonstrates capabilities and deficiencies considering the presumptions:

- The retrieval algorithm is applicable to synthetic radar reflectivity measurements.
- The singular case of the LSE remains as an issue for two observing radars.
- Local perturbations of the observations, e.g. clutter, have a local impact on the solution.

- Missing attenuating values within the LSE lead to the underestimation of the solution.
- Moderate, expected noise results in a robust solution.
- A bias in the radar's calibration can result in fluctuations in the solution.
- A well-calibrated weather radar network is mandatory.
- The uncertainty occurs at the rain area edges in the first place.
- Increasing the number of independent information, e.g. from additional radars, stabilises the solution.
- An ill-suited interpolation method manipulating the data introduces uncertainty to the solution.
- Patterns with strong attenuation lose small observed reflectivities and thus possibly relevant information.

Notwithstanding the limitations of the LSE-method, the retrieval of reflectivity and attenuation on real radar data is applied and discussed in Chapter 5.

5 Application of the Retrieval Algorithm on Real Radar Data

The applicability of the LSE-method to retrieve reflectivity and specific attenuation by using real weather radar observations has not yet been shown. Still, the synthetic radar data already approximates real conditions (Chap. 4), and thus shows limitations by measuring errors and potentiality by accurate results. The assumptions of the synthetic data and LSE-method have to be noted:

- The vertical reflectivity profile is constant.
- The intrinsic reflectivity is equal for the same nodes.
- The observations are simultaneous.

With real observations, uncertainties are investigated and outlined. The weather radar network of PATTERN provides a series of simultaneous measurements by X-band weather radars and MRRs. The weather radars HWT, MOD, and BKM are taken into account for the retrieval due to the network's structure. The three radars are the closest radars out of the network of the four weather radars. With a radius of 20 km each, the radars span an overlapping area of roughly 1200 km^2. Based on the observations of a selected case, the results of the retrieval algorithm are discussed.

Exemplary observed reflectivities Z' from the 15.05.2013 15:45:00 UTC are considered (Fig. 5.1). The selected case includes a spacious rain area with high reflectivities in parts indicating strong rain rates. Consequently, nodes of high reflectivities are affected by strong attenuation (Chap. 2). The radar data is cleaned from noise, clutter, and is calibrated with MRR-observations as described by Lengfeld et al. (2014). The data preprocessing reduces the errors of the observations but lacks the correction of attenuation. The maxima of the measured reflectivities of the weather radars are $\max(Z'_{\mathrm{HWT}}) = 55.01\,\mathrm{dBZ}$, $\max(Z'_{\mathrm{MOD}}) = 56.47\,\mathrm{dBZ}$, and $\max(Z'_{\mathrm{BKM}}) = 51.52\,\mathrm{dBZ}$. Additionally, the simultaneous measurements partially show structural similarities, e.g. the high reflectivity in the south of the radar site MOD. Nevertheless, the amplitudes of Z' appear to be different (Fig. 5.1). Missing values within the observation occur in the near field of the radar. A further notable structural difference is the high reflectivity area in the south of the overlapping area. The radar BKM can not observe this

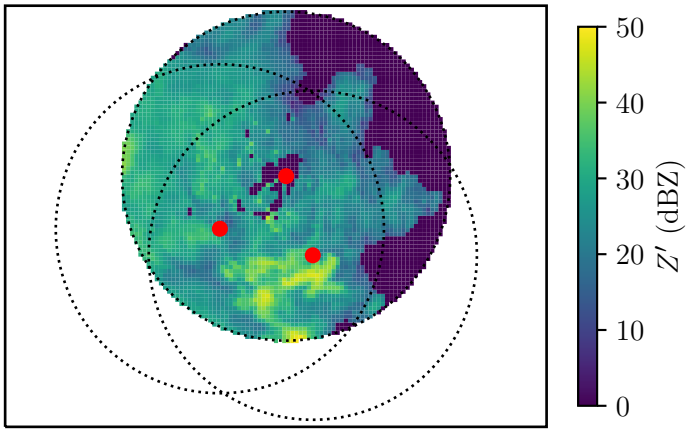

(a) Radar HWT.

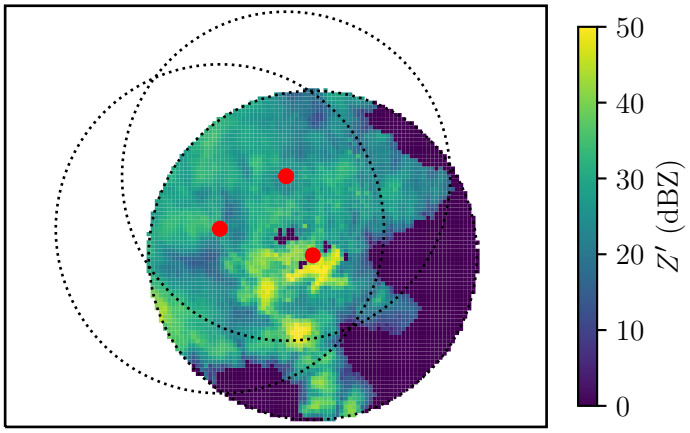

(b) Radar MOD.

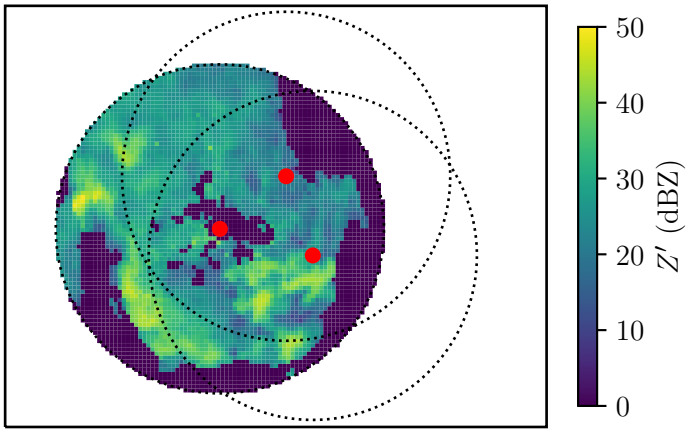

(c) Radar BKM.

Figure 5.1: Exemplary observed reflectivities Z' of the PATTERN weather radar network, 15.05.2013 15:45:00 UTC. The values are interpolated on the Cartesian model domain. The red dots indicate the three radar sites HWT (north), MOD (south east), and BKM (west). The dotted lines show the 20 km radius of the respective radar. Z' is calibrated, noise-, and clutter-free. Missing values are also shown as 0 dBZ.

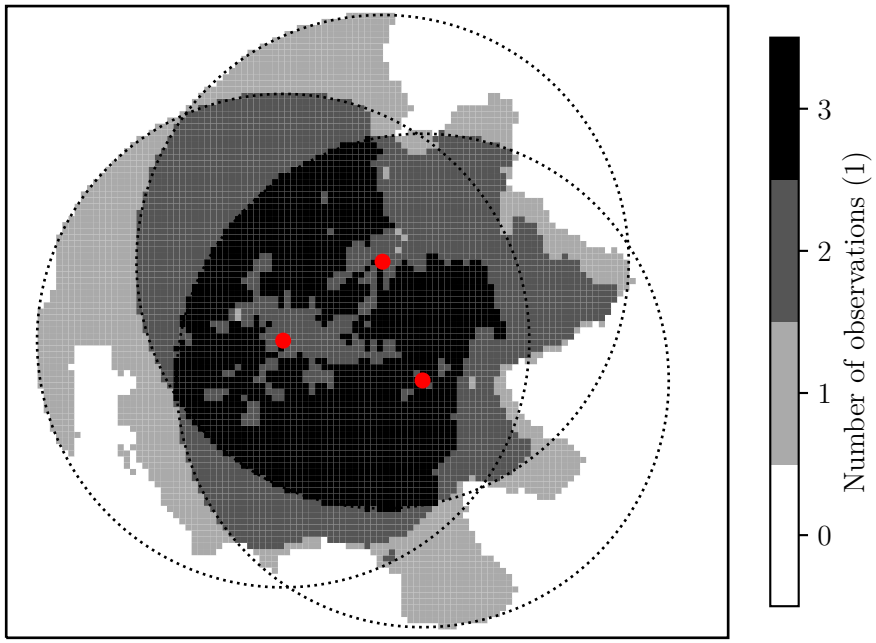

Figure 5.2: Map of simultaneous observed reflectivities Z' greater than 0 dBZ, 15.05.2013 15:45:00 UTC. The red dots indicate the three radar sites of PATTERN: HWT (north), MOD (south east), and BKM (west). The dotted lines show the 20 km radius of the respective radar.

high reflectivity event, whereas the radars HWT and MOD measure reflectivities about 50 dBZ. In summary, uncertainties characterise the observations of the weather radar network. On the one hand, the three radars measure different reflectivities as expected by the presence of attenuation. On the other hand, the weather radars observe different extents of the same rain area (Fig. 5.2). Within the overlapping area, 99.1% of the nodes are measured with a reflectivity greater than 0 dBZ by at least one weather radar, 97.1% by at least two weather radars, but only only 65.0% by all three radars. The factors that could impact the observations and thus the quality of the retrieval are discussed in detail within this chapter. Firstly, the LSE-method is applied on the real weather radar data within the network (Fig. 5.3).

The LSE-method results in the radar reflectivity $\widehat{Z}$ (Fig 5.3a) and specific attenuation $\widehat{k}$ (Fig 5.3b) for the observations from the 15.05.2013 15:45:00 UTC. Following the theoretical background of the LSE-method, quantities can only be retrieved for nodes where all three radars have valid measurements (Chap. 3). Consider a node with a measured reflectivity Z' greater than 0 dBZ observed by at least one radar as a potentially rainy node. As a result, only for 65.5% of these nodes the retrieval can be applied. Apparently, the retrieval algorithm lacks information from missing rainy nodes (Fig. 5.3). Nevertheless, the retrieved radar reflectivity $\widehat{Z}$ shows a recognisable structure compared to the observed reflectivities Z' (Fig. 5.3a). Contrarily, at the retrieved

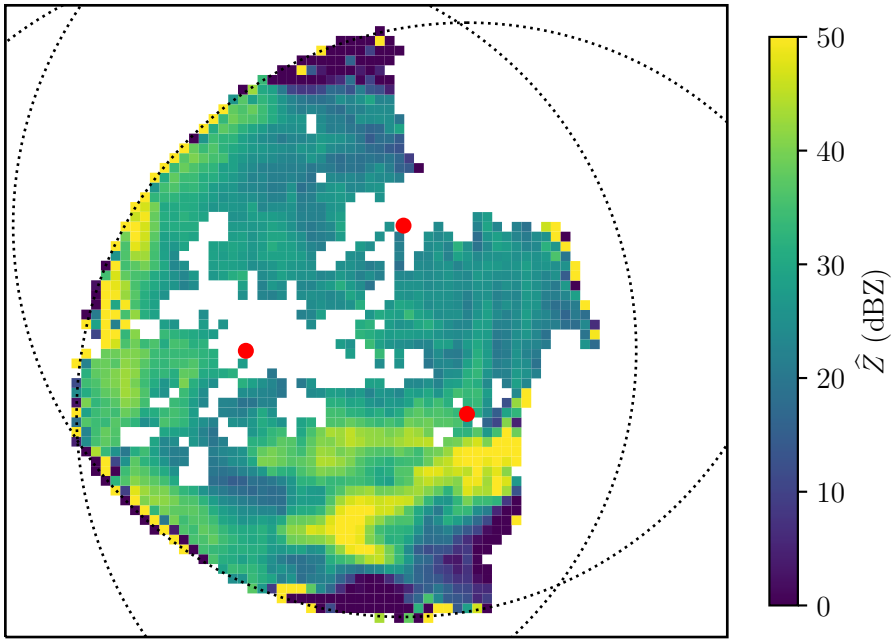

(a) Radar reflectivity.

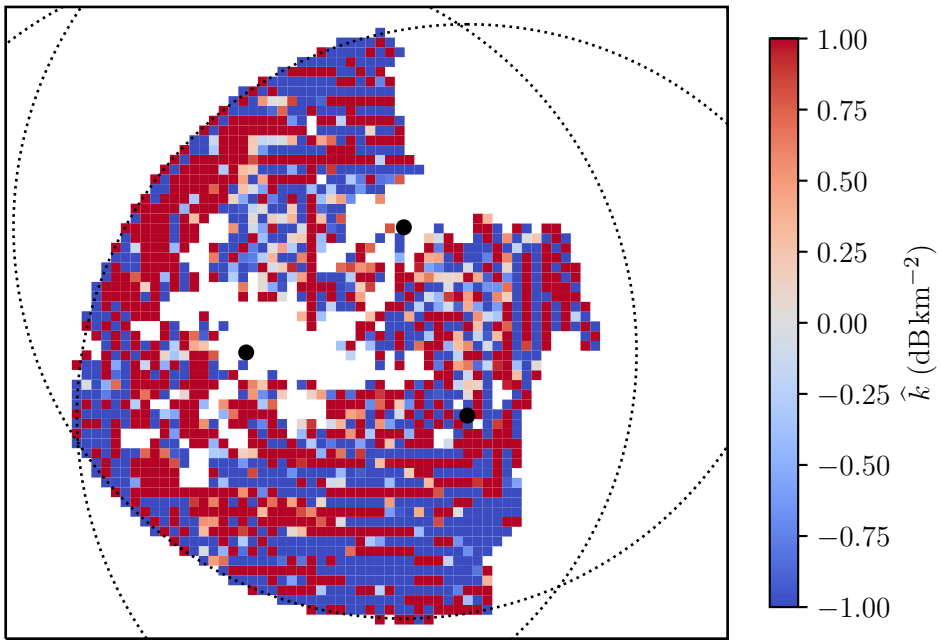

(b) Specific attenuation.

Figure 5.3: Retrieval of exemplary observed reflectivity Z' of the PATTERN weather radar network, 15.05.2013 15:45:00 UTC. The red dots indicate the three radar sites of PATTERN: HWT (north), MOD (south east), and BKM (west). The dotted lines show the 20 km radius of the respective radars.

area's edges, unphysical high reflectivities and reflectivity gradients are retrieved. The described high reflectivity event, which is observed by the radars HWT and MOD, but not BKM, results in high negative reflectivities and thus the intrinsic reflectivity Z is lost. With Equation 2.1, the difference between the retrieved and observed reflectivity $\widehat{Z} - Z'$ leads to a retrieved $\widehat{PIA}$. The intrinsic PIA for the three radar observations is physically always positive, but this retrieved $\widehat{PIA}$ is also negative in parts. Overall, the retrieved reflectivity $\widehat{Z}$ is not the expected intrinsic reflectivity Z. The expected intrinsic reflectivity Z is a continuous reflectivity field, comparable to a Gaussian field. Unlike the retrieved reflectivity $\widehat{Z}$, the retrieved specific attenuation $\widehat{k}$ is characterised by fluctuations. $\widehat{k}$ is positive and negative without apparent structure. In summary, the retrieval algorithm is not applicable to this case. To clarify, the factors impacting the quality of the retrieval are discussed in detail.

First of all, clutter reduces the quality of the retrieval. The measurements lack values in the radars' near field because of clutter induced by the ground. Because of the clutter removal, the area of observed reflectivities is not closed. Due to the number of missing values, the interpolation is not able to restore these areas. The missing values lead to the underestimation of the PIA as described in Section 4.3.

Additionally, the attenuation leads to structural differences based on missing or low values. Strong attenuation can lead to blind spots if the backscattered signal is too weak. Exemplarily, the radar BKM can not observe the high reflectivity event in the south of the overlapping area, whereas the radars HWT and MOD measure reflectivities about 50 dBZ. This observation is probably based on the PIA. Over the path, areas with reflectivities over 35 dBZ attenuate the radar signal. In summary, strong attenuation may result in missing or too low values and thus decreases the quality of the retrieval algorithm.

Even though strong attenuation and clutter are factors that reduce the retrieval's quality, noise induced by the atmosphere and internal electronics is not expected to be an issue. In general, the noise level is estimated from a rain-free measurement. In detail, if more than 10% of the radar range gates detect no rain after subtracting an initial guess from the original measurement, the 10th percentile of the original measurement is chosen as the noise level (Lengfeld et al., 2014). This noise level is spatially independent and subtracted from the observed reflectivity. Measurements of the PATTERN radar network, taken on the 15.05.2013 between 11:00:00 UTC and 19:59:30 UTC, are investigated. The estimated noise levels by the method from Lengfeld et al. (2014) are in the order of $10^{-7}\,\mathrm{mm^6\,m^{-3}}$. This noise level does not modify relevant reflectivities at all. As an example, a small rain rate of $R = 0.1\,\mathrm{mm\,h^{-1}}$ results with Equation 4.3 in $z = 15.9\,\mathrm{mm^6\,m^{-3}}$, or 12.0 dBZ. The subtraction of the noise level from the reflectivity is not relevant within this magnitude. With another

point of view on the observation's noise, Jacob (2016) applied a simple, fast noise variance estimation by Immerkaer (1996). The noise is estimated depending whether the measurements are rainy or rain-free. Jacob (2016) proposes that the mean image noise of reflectivity is about 0.5 dB for the PATTERN radars. This mean image noise as a hypothetical noise of the observation can increase the bias and RMSE of the results (Fig. 4.7). However, this mean image noise probably overestimates the observation's noise. Immerkaer (1996) limits the applicability of this noise variance estimation for highly textured images, which includes weather radar observations. Overall, noise is a minor factor doe not affect the quality of this retrieval.

Retrieval methods based on weather radar networks suffer especially from geometrical aspects. Chandrasekar and Lim (2008) mentioned the range resolution volume mismatch and pointing mismatch for common volumes. The intrinsic reflectivity is assumed to be equal at same nodes for all radars. The observation volumes can be different due to the beam expansion and beam angle. Because the distribution of rainfall is commonly non-uniform, this results in a range resolution volume mismatch. The error can be minimised for small resolution volumes. Further, azimuth misalignment of the radar leads to a pointing mismatch spatially. Different nodes are compared because the radars are spatially apart. Additionally, the scanning geometry results in different measuring heights due to the beam width and elevation angle (Jacob, 2016). Nevertheless, the LSE-method and elevation are based on a strong restriction. The vertical microphysical properties of the precipitating area are assumed to be approximately constant or the elevation angle of the radars is nearly zero. The elevation angles of the radars are roughly 3°. The measuring heights, defined as the mean beam height of the three radars, are in the range from 11 m for the radar BKM at the radar site to 1086 m for the radar HWT in maximal distance. The absolute difference of the mean beam heights are a measure for the vertical pointing error (Fig 5.4). The maximum of the absolute difference of the mean beam heights is 1235 m. The vertical pointing error is not relevant if the vertical microphysical properties of the precipitation can be assumed to be constant. For this case, different measuring heights would result in the same reflectivities for the same nodes. Generally, for mean vertical profiles, reflectivity is assumed to be constant between the surface and the melting layer[1] (Peters et al., 2010). Peters et al. (2010) found a significant height dependence of the reflectivity at high rain rates by measuring the DSD. The vertical inhomogeneity is physically reasonable because of the enhanced probability of raindrop collisions in high rain rates (Peters et al., 2010). Based on the assumptions for the LSE-method, this implicates a backlash. Since PATTERN includes MRR measurements, a vertical profile for the

[1] The level where the hydrometeors are in the phase transition between ice and water (Doviak and Zrnić, 1993).

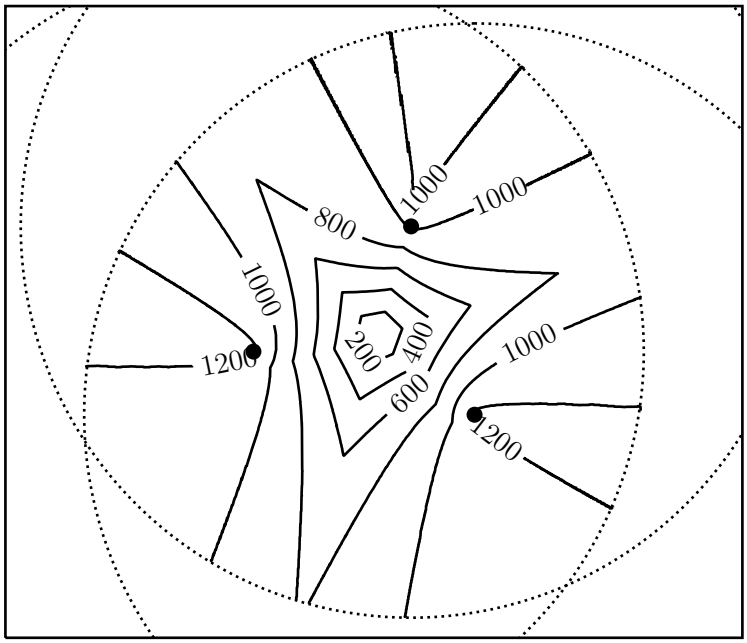

Figure 5.4: Cumulated, absolute difference of the beam heights of the three radars in meters. The dots indicate the three radar sites of PATTERN: HWT (north), MOD (south east), and BKM (west). The dotted lines show the 20 km radius of the respective radar.

selected case of Figure 5.1 is available. Consistent with the time of the observation, 10 s-measurements are investigated (Fig. 5.5). The detailed reflectivity profile shows a significant height dependence. The vertical reflectivity varies between 21.61 dBZ and 28.37 dBZ, thus a difference up to 6.71 dB. On the one hand, the radars HWT and MOD observe the location of the MRR WST in the same height and extent. On the other hand, the radar BKM observes this location in a lower altitude. The radar BKM observes a fully different volume than the radars HWT and MOD. The different observation heights result in a bias between the individual radar measurements. The impact of a bias superimposing the measurements on the retrieval is discussed in detail in Chapter 4 and Figure 4.10. Additionally, Jacob (2016) already outlines the geometrical induced uncertainty of measurements. The investigation of two theoretical weather radars identical to the PATTERN radars with a 2° elevation angle and MRR measurements demonstrates significant deviations in the measured reflectivities. These radars measure between 60% more or 45% less reflectivity at the same location than a second radar for different beam heights (Jacob, 2016). These differences have an impact on the retrieval results (Fig. 4.10). In sum, the scanning strategy and vertical inhomogeneity of the reflectivity are the major factors affecting the quality of the retrieval. The erroneous assumption impedes the LSE-method to be successful for the weather radar network of PATTERN.

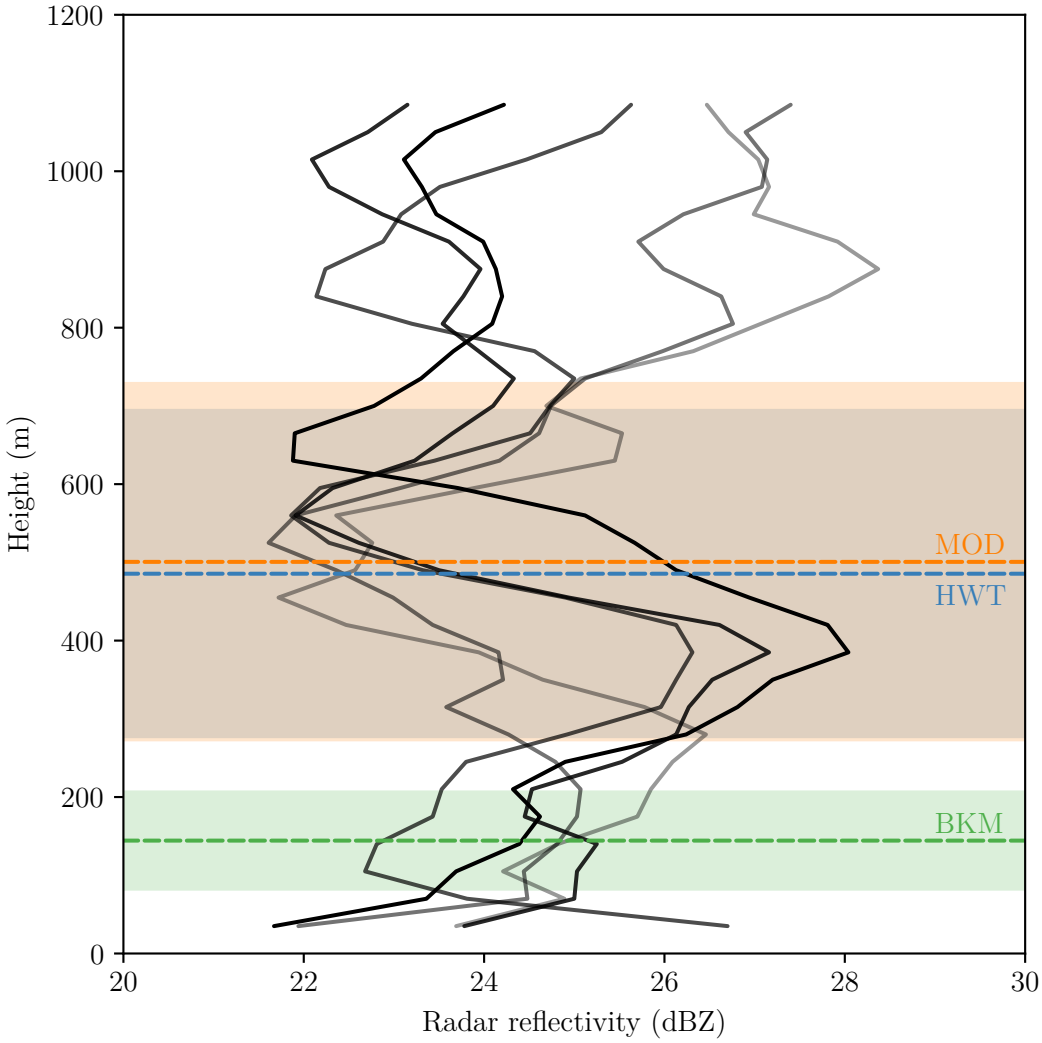

Figure 5.5: Five exemplary vertical profiles of the radar reflectivity Z observed by the MRR WST consistent with the observation time of Figure 5.1, 15.05.2013 15:45:47 to 15:46:27 UTC. The dashed lines shows the mean beam height of the three radars HWT, MOD, and BKM. The shaded area indicates the beam height including the beam width.

All in all, the application of the LSE-method on real radar data demonstrates the drawbacks that come along with real measurements:

- Ground clutter and strong attenuation cause missing values, underestimating the *PIA*.
- Strong attenuation can weaken the backscattered signal, which can not be resolved with the LSE.
- Noise has an insignificant magnitude and does therefore not affect the LSE solution.
- Range resolution volume and pointing mismatches result in different measurements for same nodes.
- The measured reflectivities are incomparable in part due to the scanning strategy and vertical inhomogeneity of the reflectivity.

The novel retrieval method can not estimate reflectivity and specific attenuation in the PATTERN weather radar network. Notwithstanding, the applicability of the LSE-method to weather radar networks with other geometries or microwave link applications is not excluded.

6 Conclusion and Outlook

The concept of a weather radar network providing multiple information about same measuring volumes is a possible basis to overcome the drawback of attenuation. The observation of intrinsic reflectivity for a common volume is distinct due to different integrated attenuation along the paths from each radars and additional uncertainties. Therefore, a novel retrieval method for reflectivity and specific attenuation estimates in weather radar networks has been presented, the LSE-method. The networked observations are considered as a tomographic problem. The retrieval methodology is the least square solution of a determined or overdetermined linear system of equations derived from multiple observations. The LSE-method makes direct use of the physical equation relating the intrinsic reflectivity, observed reflectivity, and the specific attenuation integrated over the path. A major advantage of this method compared to other attenuation correction schemes is the solution's independence of constraints and statistical relations, like the k-Z-relation. Furthermore, the retrieval method can be easily applied to a weather radar network of even two or multiple radars. Due to the physical background, the radar sites have to be located within the model domain. Consequently, the technique requires a special network design. Additionally, the vertical microphysical properties in form of the reflectivity are assumed to be approximately constant or the elevation angle of the radars nearly zero. Simultaneous measurements are required. More specifically, the intrinsic reflectivities of the weather radars have to be equal on condition.

The retrieval algorithm is first tested using synthetic weather radar data to prove the validity and sensitivity of the method. The synthetic data allows to have simultaneous observations and separates the impact of attenuation and different uncertainties. Several setups with different complexity are investigated by two or three radars: a constant one-, two-dimensional box precipitation, and realistic structured two-dimensional Gaussian precipitation. The isolated uncertainties, e.g. noise, clutter or a calibration bias, are superimposed on the synthetic observations. The sensitivity of the LSE-method is discussed for local perturbations, noise, missing values, biases, different number of radars, and strong attenuation. Especially a noise significant greater than the specific attenuation and biases between the observed reflectivities corrupt the retrieval's solution. The LSE-method is found to be applicable to synthetic data of weather radar

networks considering the underlying assumptions of the observations.

Due to the promising results of the synthetic study, the retrieval algorithm was studied on a real world rain event. The radars of the project PATTERN provide these real observations. The real radar data turns out to misfit the theoretical assumptions. The measured reflectivities are incomparable in part due to the scanning strategy and vertical inhomogeneity of the reflectivity. The radar's scanning strategy leads to different measuring heights and volumes. Further, the reflectivity varies with height. In combination, these characteristics are inconsistent with the presumptions of the LSE-method. In addition, ground clutter and strong attenuation causes missing values in the observations. The spacious measurements of the networked radars are inconsistent. For example, the radars only agree on a reflectivity greater than 0 dBZ in two-thirds of the overlapping area for the investigated rain event. The path integrated specific attenuation is underestimated by these uncertainties. Contrarily, the noise of the PATTERN radars has an insignificant magnitude not affecting the retrieval. Unfortunately, the PATTERN weather radars do not provide comparable reflectivity data for the application of the LSE-method.

The advice for prospective attenuation correction schemes for weather radar networks is to compare intersecting volumes explicitly. The attenuation correction of the single-polarised X-band weather radars of PATTERN is evidently challenging. Nevertheless, PATTERN can benefit by the synergy of horizontal, low-elevation X-band radars with vertical pointing MRRs. Other weather radar networks consist of polarised weather radars operating at multiple elevation, like C-band radars of the DWD, can make use of more comparable volumes and polarisation.

Consistently, the application of the LSE-method to retrieve reflectivity and specific attenuation is constrained to a weather radar network operating at zero elevation. Merker (2013) describes an experimental setup for radars along connecting lines. In further study, the observations made by this framework might validate the retrieval method for real radar data. Unfortunately, the measurements also show inconsistencies due to the setup of elevation and the beam expansion.

However, the fundamental analysis of the presented method to retrieve reflectivity and specific attenuation in a weather radar network proves its theoretical validity. The method could offer opportunities for attenuation correction of radar networks operating in strongly attenuated frequency ranges, providing accurate and comparable data for application. Overall, the research on attenuation correction schemes for weather radars operating at small wavelengths has still not been completed. Weather radar networks are capable to improve rain estimates considering the measurement's background.

Bibliography

Abrahamsen, P. (1997). *A review of Gaussian random fields and correlation functions.*

Antonini, A., S. Melani, M. Corongiu, S. Romanelli, A. Mazza, A. Ortolani, and B. Gozzini (2017). "On the implementation of a regional X-band weather radar network". In: *Atmosphere* 8.2, p. 25.

Aster, R. C., B. Borchers, and C. H. Thurber (2013). *Parameter estimation and inverse problems.* Elsevier. DOI: 10.1016/C2009-0-61134-X.

Atlas, D. and H. C. Banks (1951). "The interpretation of microwave reflections from rainfall". In: *Journal of Meteorology* 8.5, pp. 271–282.

Atlas, D. and C. W. Ulbrich (1977). "Path-and area-integrated rainfall measurement by microwave attenuation in the 1–3 cm band". In: *Journal of Applied Meteorology* 16.12, pp. 1322–1331.

Austin, P. M. (1947). "Measurement of approximate raindrop size by microwave attenuation". In: *Journal of Meteorology* 4.4, pp. 121–124.

Berne, Alexis and Witold F Krajewski (2013). "Radar for hydrology: Unfulfilled promise or unrecognized potential?" In: *Advances in Water Resources* 51, pp. 357–366.

Burgemeister, F. (2018). "Kalibration eines Radar-Netzwerkes mit Hilfe der Sonne". Bachelor's thesis.

Chandrasekar, V., H. Chen, and B. Philips (2018). "Principles of high-resolution radar network for hazard mitigation and disaster management in an urban environment". In: *Journal of the Meteorological Society of Japan. Ser. II* 96, pp. 119–139.

Chandrasekar, V. and S. Lim (2008). "Retrieval of reflectivity in a networked radar environment". In: *Journal of Atmospheric and Oceanic Technology* 25.10, pp. 1755–1767.

Cifelli, R., V. Chandrasekar, H. Chen, and L. E. Johnson (2018). "High resolution radar quantitative precipitation estimation in the San Francisco Bay area: rainfall monitoring for the urban environment". In: *Journal of the Meteorological Society of Japan. Ser. II* 96, pp. 141–155.

Delrieu, G., L. Hucke, and J. D. Creutin (1999). "Attenuation in rain for X-and C-band weather radar systems: Sensitivity with respect to the drop size distribution". In: *Journal of Applied Meteorology* 38.1, pp. 57–68.

Doviak, R. J. and D. S. Zrnić (1993). *Doppler Radar and Weather Observations*. Mineola, New York: Dover Publications.

Einfalt, T. (2003). "A user perspective in Germany: What is expected by agencies and government from radar data?" In: *International Journal of River Basin Management* 1.3, pp. 199–203.

Feng, L., H. Xiao, G. Wen, Z. Li, Y. Sun, Q. Tang, and Y. Liu (2016). "Rain attenuation correction of reflectivity for X-band dual-polarization radar". In: *Atmosphere* 7.12, p. 164.

Gunn, K. L. S. and T. W. R. East (1954). "The microwave properties of precipitation particles". In: *Quarterly Journal of the Royal Meteorological Society* 80.346, pp. 522–545.

Hildebrand, P. H. (1978). "Iterative correction for attenuation of 5 cm radar in rain". In: *Journal of Applied Meteorology* 17.4, pp. 508–514.

Hitschfeld, W. and J. Bordan (1954). "Errors inherent in the radar measurement of rainfall at attenuating wavelengths". In: *Journal of Meteorology* 11.1, pp. 58–67.

Immerkaer, J. (1996). "Fast noise variance estimation". In: *Computer vision and image understanding* 64.2, pp. 300–302.

Jacob, M. (2016). "Uncertainties of C- and X-Band Radar Measurements – Theoretical Quantifications". Master's thesis.

Kabèche, A. and J. Testud (1995). "Stereoradar meteorology: A new unified approach to process data from airborne or ground-based meteorological radars". In: *Journal of Atmospheric and Oceanic Technology* 12.4, pp. 783–799.

Lengfeld, K., M. Berenguer, and D. S. Torres (2018). "Intercomparison of attenuation correction algorithms for single-polarized X-band radars". In: *Atmospheric Research* 201, pp. 116–132.

Lengfeld, K., M. Clemens, C. Merker, H. Münster, and F. Ament (2016). "A simple method for attenuation correction in local X-band radar measurements using C-band radar data". In: *Journal of Atmospheric and Oceanic Technology* 33.11, pp. 2315–2329.

Lengfeld, K., M. Clemens, H. Münster, and F. Ament (2014). "Performance of high-resolution X-band weather radar networks – the PATTERN example". In: *Atmos. Meas. Tech.* 7, pp. 4151–4166. DOI: 10.5194/amt-7-4151-2014.

Lim, S., V. Chandrasekar, P. Lee, and A. P. Jayasumana (2011). "Real-time implementation of a network-based attenuation correction in the CASA IP1 testbed". In: *Journal of atmospheric and oceanic technology* 28.2, pp. 197–209.

Marzoug, M. and P. Amayenc (1991). "Improved range-profiling algorithm of rainfall rate from a spaceborne radar with path-integrated attenuation constraint". In: *IEEE Transactions on Geoscience and Remote Sensing* 29.4, pp. 584–592.

Merker, C. (2013). “A Novel Approach for Absolute Calibration of Radars”. Master’s thesis.

Nicol, J. C. and G. L. Austin (2003). “Attenuation correction constraint for single-polarisation weather radar”. In: *Meteorological Applications* 10.4, pp. 345–354.

Ochoa-Rodriguez, S., L.-P. Wang, A. Gires, R. D. Pina, R. Reinoso-Rondinel, G. Bruni, A. Ichiba, S. Gaitan, E. Cristiano, J. van Assel, et al. (2015). “Impact of spatial and temporal resolution of rainfall inputs on urban hydrodynamic modelling outputs: A multi-catchment investigation”. In: *Journal of Hydrology* 531, pp. 389–407.

Paige, C. and M. Saunders (1982). “LSQR: An algorithm for sparse linear equations and sparse least squares”. In: *ACM Transactions on Mathematical Software (TOMS)* 8.1, pp. 43–71.

Peters, G., B. Fischer, and M. Clemens (2010). “Rain attenuation of radar echoes considering finite-range resolution and using drop size distributions”. In: *Journal of atmospheric and Oceanic Technology* 27.5, pp. 829–842.

Powell, C. E. et al. (2014). “Generating realisations of stationary gaussian random fields by circulant embedding”. In: *matrix* 2.2, p. 1.

Shimamura, S., V. Chandrasekar, T. Ushio, G. Kim, E. Yoshikawa, and H. Chen (2016). “Probabilistic attenuation correction in a networked radar environment”. In: *IEEE Transactions on Geoscience and Remote Sensing* 54.12, pp. 6930–6939.

Srivastava, R. C. and L. Tian (1996). “Measurement of attenuation by a dual-radar method: Concept and error analysis”. In: *Journal of Atmospheric and Oceanic Technology* 13.5, pp. 937–947.

Testud, J. and P. Amayenc (1989). “Stereoradar meteorology: A promising technique for observation of precipitation from a mobile platform”. In: *Journal of Atmospheric and Oceanic Technology* 6.1, pp. 89–108.

Thorndahl, S., T. Einfalt, P. Willems, J. E. Nielsen, M.-C. ten Veldhuis, K. Arnbjerg-Nielsen, M. R. Rasmussen, and P. Molnar (2017). “Weather radar rainfall data in urban hydrology”. In: *Hydrology and Earth System Sciences* 21.3, pp. 1359–1380.

Tian, L. and R. C. Srivastava (1997). “Measurement of attenuation at C band in a convective storm by a dual-radar method”. In: *Journal of Atmospheric and Oceanic Technology* 14.1, pp. 184–196.

Van de Beek, C. Z., H. Leijnse, J. N. M. Stricker, R. Uijlenhoet, and H. W. J. Russchenberg (2010). “Performance of high-resolution X-band radar for rainfall measurement in The Netherlands”. In: *Hydrology and Earth System Sciences* 14.2, pp. 205–221.

Wexler, R. and D. Atlas (1963). “Radar reflectivity and attenuation of rain”. In: *Journal of Applied Meteorology* 2.2, pp. 276–280.

Xu, Jinchao and Ludmil Zikatanov (2017). “Algebraic multigrid methods”. In: *Acta Numerica* 26, pp. 591–721.

List of Figures

2.1 Sketch of a radar network observing the same volume. 5
2.2 Map of weather radar network PATTERN. 6

3.1 Idealised set up of a radar network along connecting lines. 11
3.2 Discretisation of fields using a nodal finite element basis. 13
3.3 Weighting of two beam paths on a two-dimensional field using the nodal element basis. 14

4.1 Outline for evaluating the retrieval method using synthetic data. 20
4.2 Synthetic one-dimensional box precipitation. 21
4.3 Synthetic two-dimensional box precipitation. 23
4.4 Synthetic two-dimensional Gaussian precipitation. 24
4.5 Retrieval on synthetic one-dimensional box precipitation with superimposed local perturbations. 26
4.6 Retrieval on synthetic one-dimensional box precipitation with superimposed noise. 27
4.7 Ensemble of the retrieval on synthetic one-dimensional box precipitation with superimposed noise. 29
4.8 Retrieval on two-dimensional box precipitation observed by two radars. 30
4.9 Retrieval on two-dimensional box precipitation observed by three radars biased by a calibration error. 32
4.10 Ensemble of the retrieval on synthetic one-dimensional box precipitation with superimposed calibration bias. 33
4.11 Distribution between the observed and intrinsic radar reflectivity of a two-dimensional precipitation area based on Gaussian random fields. . . 35
4.12 Distribution between the retrieved and intrinsic quantities of a two-dimensional precipitation area based on Gaussian random fields. 36

5.1 Exemplary observed reflectivities of the PATTERN weather radar network. 40
5.2 Map of simultaneously observed reflectivities. 41
5.3 Retrieval method applied on observed reflectivity of the PATTERN weather radar network. 42
5.4 Beam height differences of the PATTERN weather radar network. . . . 45

5.5 Vertical profile of radar reflectivity. 46

Danksagung

An dieser Stelle möchte ich mich bei allen bedanken, die mich im vergangenen Jahr motiviert und unterstützt haben diese Masterarbeit zu schreiben.
Besonderer Dank gilt Dr. Marco Clemens, der sich, mit einer offenen Tür, immer wieder Zeit für Gespräche inklusive zielführender Diskussionen genommen hat. Die von ihm angebotenen wöchentlichen Besprechungen haben die Arbeit maßgeblich vorangebracht.
Ein großer Dank geht an Prof. Dr. Felix Ament für die Idee dieser Arbeit, die sehr gute Betreuung und das große Interesse bei Unklarheiten.
An meine Freundinnen und Freunde, Kommilitoninnen und Kommilitonen: Vielen Dank für die gemeinsame Zeit!
Bei Tobias Finn und Tobias Machnitzki möchte ich mich für ein produktives Arbeiten und die großartige Stimmung im gemeinsamen Büro bedanken. Die Anmerkungen von Tobias Machnitzki zur Korrektur meiner gesamten Arbeit haben diese sprachlich und fachlich verbessert. Die zahlreichen Diskussionen mit Tobias Finn waren fachlich wertvoll und nicht-fachlich unterhaltsam.
Außerdem möchte ich Katharina Baier, Tobias Finn, Henning Franke, Lara Hellmich, Daniel Krieger, Tobias Machnitzki, Julia Menken und Moritz Witt für die Korrektur von Abschnitten meiner Arbeit danken.
Ich möchte mich bei der gesamten Arbeitsgruppe „Atmosphärenmessungen / Prozessmodellierung“ für die sehr gute Arbeitsatmosphäre bedanken. Ich freue mich auf die weitere Zusammenarbeit mit Prof. Dr. Felix Ament, Dr. Marco Clemens und der Arbeitsgruppe.
Zu guter Letzt möchte ich meiner Familie danken, die mir das Studium ermöglicht hat.

Versicherung an Eides statt

Hiermit versichere ich an Eides statt, dass ich die vorliegende Arbeit im Studiengang Meteorologie selbstständig verfasst und keine anderen als die angegebenen Hilfsmittel – insbesondere keine im Quellenverzeichnis nicht benannten Internet-Quellen – benutzt habe. Alle Stellen, die wörtlich oder sinngemäß aus Veröffentlichungen entnommen wurden, sind als solche kenntlich gemacht. Ich versichere weiterhin, dass ich die Arbeit vorher nicht in einem anderen Prüfungsverfahren eingereicht habe und die eingereichte schriftliche Fassung der auf dem elektronischen Speichermedium entspricht.
Zusätzlich bin ich mit der Ausstellung der Arbeit in der Fachbibliothek einverstanden.

Hamburg, den 20. Februar 2020